Received: 15 May 2019 | Revised: 3 March 2020 | Accepted: 26 March 2020

DOI: 10.1096/fj.201901195RRR

RESEARCH ARTICLE

THE FASEB JOURNAL

KCTD5, a novel TRPM4-regulatory protein required for cell migration as a new predictor for breast cancer prognosis

José Rivas[1,2,3] | Nicolás Díaz[1,2] | Ian Silva[1,2] | Danna Morales[2,4] | Boris Lavanderos[1,2] | Alhejandra Álvarez[1,2] | María Paz Saldías[1,2] | Eduardo Pulgar[5] | Pablo Cruz[1,2] | Diego Maureira[1,2] | Guillermo Flores[1] | Alicia Colombo[6,7] | Constanza Blanco[1,2] | Héctor R. Contreras[6] | Fabián Jaña[3,8] | Ivan Gallegos[6,7] | Miguel L. Concha[5,9,10,11] | Ariela Vergara-Jaque[2,12,13] | Horacio Poblete[2,12,13] | Wendy González[2,13] | Diego Varela[2,4] | James S. Trimmer[14] | Mónica Cáceres[1,2,8] | Oscar Cerda[1,2,8]

[1]Program of Cellular and Molecular Biology, Institute of Biomedical Sciences (ICBM), Faculty of Medicine, Universidad de Chile, Santiago, Chile

[2]Millennium Nucleus of Ion Channel-Associated Diseases (MiNICAD), Santiago, Chile

[3]Departamento de Ciencias de la Salud, Universidad de Aysén, Coyhaique, Chile

[4]Program of Physiology and Biophysics, Institute of Biomedical Sciences (ICBM), Faculty of Medicine, Universidad de Chile, Santiago, Chile

[5]Program of Anatomy and Developmental Biology, Institute of Biomedical Sciences (ICBM), Faculty of Medicine, Universidad de Chile, Santiago, Chile

[6]Departamento de Oncología Básico Clínica, Faculty of Medicine, Universidad de Chile, Santiago, Chile

[7]Departamento de Anatomía Patológica, Hospital Clínico Universidad de Chile, Universidad de Chile, Santiago, Chile

[8]The Wound Repair, Treatment and Health (WoRTH) Initiative, Santiago, Chile

[9]Biomedical Neuroscience Institute, Santiago, Chile

[10]Center for Geroscience, Brain Health and Metabolism, Santiago, Chile

[11]Millennium Nucleus on Physics of Active Matter, Santiago, Chile

[12]Multidisciplinary Scientific Nucleus, Universidad de Talca, Talca, Chile

[13]Center for Bioinformatics and Molecular Simulations (CBSM), Faculty of Engineering, Universidad de Talca, Talca, Chile

[14]Department of Physiology and Membrane Biology, School of Medicine, University of California, Davis, CA, USA

Correspondence
Oscar Cerda, Program of Cellular and Molecular Biology, Institute of Biomedical Sciences (ICBM), Faculty of Medicine, Universidad de Chile, Santiago, Chile.
Email: oscarcerda@uchile.cl

Funding information
Fondo Nacional de Desarrollo Científico y Tecnológico (FONDECYT), Grant/Award Number: 1160518, 11170291, 11170223, 1171155, 1190806, 1160900 and 1181263; Iniciativa Científica Milenio

Abstract

Transient receptor potential melastatin 4 (TRPM4) is a Ca^{2+}-activated nonselective cationic channel that regulates cell migration and contractility. Increased TRPM4 expression has been related to pathologies, in which cytoskeletal rearrangement and cell migration are altered, such as metastatic cancer. Here, we identify the K^+ channel tetramerization domain 5 (KCTD5) protein, a putative adaptor of cullin3 E3 ubiquitin ligase, as a novel TRPM4-interacting protein. We demonstrate that KCTD5 is a positive regulator of TRPM4 activity by enhancing its Ca^{2+} sensitivity. We show that through its effects on TRPM4 that KCTD5 promotes cell migration and contractility.

Abbreviations: DPBS, Dulbecco's phosphate buffered saline; ER, estrogen receptor; KCTD, K^+ channel tetramerization domain; MS, mass spectrometry; PR, progesterone receptor; shRNA, small hairpin RNA; TBS, tris-buffered saline; TRPM4, transient receptor potential melastatin 4; TNM, tumor, node, metastasis.

José Rivas, Nicolás Díaz, and Ian Silva contributed equally to this study.

[Correction added on April 28, 2020, after first online publication: The figures "Figure 1F and Figure 2A" was updated in this title and How to cite section.]

Finally, we observed that both TRPM4 and KCTD5 expression are increased in distinct patterns in different classes of breast cancer tumor samples. Together, these data support that TRPM4 activity can be regulated through expression levels of either TRPM4 or KCTD5, not only contributing to increased understanding of the molecular mechanisms involved on the regulation of these important ion channels, but also providing information that could inform treatments based on targeting these distinct molecules that define TRPM4 activity.

KEYWORDS

cell migration, KCTD proteins, TRP channels

1 | INTRODUCTION

Transient receptor potential melastatin 4 (TRPM4) is a Ca^{2+}-activated nonselective cationic channel[1] that regulates cell migration,[2-4] contractility, and wound healing.[3-5] TRPM4 localizes to focal adhesions (FA) and regulates their disassembly, leading to cytoskeletal rearrangement and altered Ca^{2+} signaling.[3,4] Increased expression of these channels has been observed in prostate cancer, B-cell non-Hodgkin lymphoma, human cervical-uterine tumor samples, and cervical-uterine cancer derived cell lines.[6-10] Moreover, increased expression of TRPM4 enhances prostate cancer cell migration.[8,11-13] As such, a better understanding of mechanisms that regulate TRPM4 activity represents a novel approach to the development of potential therapeutic strategies for these pathologies by modulating TRPM4 activity.

Potassium channel tetramerization domain (KCTD) family members are BTB (Bric-a-brac, Tramtrack, and Broad Complex) domain-containing proteins.[14] These proteins regulate diverse functions such as transcriptional repression, cytoskeletal remodeling, and ion channel gating.[14] KCTD5 is a pentameric Cullin3-RING E3 ligase-adapter protein highly expressed in spleen, thymus, testis, ovary, prostate, small, and large intestine.[15-17] Moreover, enhanced KCTD5 protein expression has been observed in transformed cell lines and peripheral blood leukocytes exposed to mitogens.[15] The *Drosophila* KCTD5 ortholog *insomniac* plays a critical role in sleep homeostasis associated with dopaminergic pathway.[18,19] In addition, KCTD5 is involved in *Helicobacter pylori* adhesion to gastric epithelial cells.[20] However, the mechanism whereby KCTD5 exerts these effects, including potential substrates and effectors of KCTD5 remain unclear.[15]

Here, we identify KCTD5 as a novel TRPM4-interacting protein that regulates TRPM4 channel activity. Moreover, we demonstrate that KCTD5 regulates cell migration and contractility through its effects on TRPM4 activity. Moreover, we found that KCTD5 is a novel regulator of cell migration in vivo. We also demonstrate that TRPM4 and KCTD5 expression is increased in breast cancer cells and tumors in distinct patterns. The expression patterns of these genes correlate with the dedifferentiation and progression characteristics of aggressive and malignant tumors. Together, these data suggest a novel role for KCTD5 as a regulator of TRPM4 activity, and that distinct modes of regulation of various TRPM4-mediated physiological and pathophysiological processes could be regulated by altered expression of TRPM4 and/or KCTD5. Our findings also suggest that both TRPM4 and KCTD5 represent attractive targets for development of drugs that modulate TRPM4 activity through these distinct mechanisms, and that which may display distinct therapeutic potential.

2 | MATERIALS AND METHODS

2.1 | Cell culture and transfections

HEK293 and COS-7 cells were cultured in DMEM high glucose medium (Thermo Fisher Scientific, Waltham, MA, USA, catalog #12100046), supplemented with 5% v/v Fetal Bovine Serum (FBS; GE Healthcare Life Sciences, Chicago, IL, USA, catalog #SV30160.03). Mouse Embryonic Fibroblasts (MEF) were maintained in DMEM high glucose medium supplemented with 10% v/v fetal bovine serum. MDA-MB-231 (ATCC HTB-26) and MCF7 (ATCC HTB-22) cells were cultured in DMEM/F12 media supplemented with 10% v/v FBS and 100 μg/mL penicillin-streptomycin. MCF10A (ATCC CRL-10317) cells were cultured in DMEM/F12 media supplemented with 5% v/v Horse Serum, 20 ng/mL EGF (Invitrogen, Carlsbad, CA, USA catalog #PHG0311), 10 μg/mL Insulin (Sigma-Aldrich, San Louis, MO, USA, catalog #I0516), and 0.5 μg/mL Hydrocortisone (Sigma-Aldrich, catalog #H0888). The T47D (ATCC HTB-133) cell line was cultured in DMEM with 5% v/v FBS. The 4T1 cell line was cultured in RPMI media supplemented with 10% v/v FBS. HEK293 and COS-7 cells were transfected with the different plasmids using Lipofectamine 2000 reagent (Thermo Fisher Scientific catalog #11668019). Mouse Embryonic Fibroblast

(MEF) cells were transfected using Lipofectamine LTX reagent (Thermo Fisher Scientific catalog #15338100). All cell lines were grown at 37°C and 5% CO_2.

HEK293 CRISPR/Cas9-based KCTD5 knockout cell line (HEK293$^{kctd5-/-}$) was generated by transfecting KCTD5-Double Nickase plasmid (h1) (Santa Cruz Biotechnology, Dallas, TX, USA, catalog #sc-409961-NIC), followed by selection with puromycin (2 μg/mL) (Thermo Fisher Scientific catalog #A1113802). Single clones were selected, and the absence of KCTD5 expression was evaluated by RT-PCR, qPCR, and immunoblot as described below.

2.2 | mRNA expression

mRNA from HEK293 and HEK293$^{kctd5-/-}$ cells was purified using TRIzol reagent (Invitrogen, catalog #15596026) according to supplier's instructions. Briefly, cells were lysed with TRIzol reagent, scraped, and centrifuged for 15 minutes at 12 000*g* at 4ºC. Next, for RNA precipitation, the aqueous phase was separated and mixed with isopropanol, incubated for 10 minutes, and centrifugated for 10 minutes at 12 000*g* at 4ºC. The pellet was resuspended in 75% v/v ethanol, vortexed briefly, and centrifuged for 5 minutes at 7500*g* at 4ºC. Finally, the obtained pellet was resuspended in DEPC-treated water and incubated at 65ºC for 10 minutes. cDNA was obtained with in vitro retrotranscription, using 1 μg of RNA sample and mixed with dNTPs (1 mM), 5X Reaction Buffer, Ribolock RNase Inhibitor (20 U) (Thermo Fisher Scientific, catalog #EO0381), Random Primers (100 pmol), and RevertAid Reverse Transcriptase (200 U) (Thermo Fisher Scientific catalog #EP0441). In vitro retrotranscription was performed using the following conditions: 25ºC for 10 minutes, 42ºC for 60 minutes, and finally, 70ºC for 10 minutes. Amplification of KCTD5 and β-actin cDNAs was carried out using the following primers (Forward/Reverse): KCTD5 (5′-GGAGCTGCTGGGATTCCTTT-3′/5′-GTCAGTCTGCACAGTACCCC-3′) 400 nM; β-actin (5′-TGACGTGGACATCCGCAAAG-3′/5′-CTGGAAG GTGGACAGCGAGG-3′) 250 nM. Quantitative PCR reactions were prepared using SensiMix SYBR Hi-ROX Kit (Bioline, London, UK catalog QT605-05) following manufacturer's instructions and reaction detection was performed using the StepOne Real-Time PCR System (Applied Biosystems, Foster City, CA, USA), using the following cycling conditions: 95°C for 10 minutes, followed by 40 cycles of 95°C for 15 seconds and 60°C for 1 minute, followed by a melt curve starting at 60°C, gradually increasing the temperature by 0.3°C to 95°C. StepOne Software v 2.3 was used for curve analyses. Relative expression was normalized to β-actin and determined using the double delta Ct method.[21] Conventional PCR was performed using Taq polymerase (Thermo Fisher Scientific catalog #EP0401) following the manufacturer's instructions. The reaction was performed on a G-STORM GS00482 Thermal cycler (G-STORM, Somerset, UK), using the following cycling conditions: 95ºC for 10 minutes, followed by 30 cycles of 95ºC for 15 s, 57.5ºC for 1 minute, and 7ºC for 1 minute. The reactions ended with a final extension step of 72ºC for 10 minutes. PCR products were resolved by electrophoresis in 2% w/v agarose gels.

2.3 | Immunoblot analyses

Cells were lysed in lysis buffer [50 mM Tris-HCl, 150 mM NaCl (Merck, Darmstadt, Germany, catalog #1064045000), 1 mM ethylenediaminetetraacetic acid (EDTA; Chemix, Lampa, Santiago, Chile, catalog #160408), 1 mM sodium orthovanadate (Calbiochem, San Diego, CA, USA, catalog #567540), 5 mM NaF (Sigma-Aldrich catalog #S7920), 1% v/v Triton X-100 (Sigma-Aldrich catalog #10789704001), pH 7.4] containing as protease inhibitors 1 mM phenylmethylsulfonyl fluoride (PMSF; Sigma-Aldrich catalog #78830) and a protease inhibitor cocktail (PIC; Cytoskeleton, Inc, Denver, CO, USA, catalog #PIC02) for 30 minutes at 4°C. The lysates were centrifuged at 12 000*g* at 4°C for 10 minutes. Reducing Sample Buffer (RSB) [62.5 mM Tris-HCl, 2% w/v SDS (Sigma-Aldrich catalog #L5750), 10% v/v glycerol (Merck catalog #356352), 1% v/v β-Mercaptoethanol (Merck catalog #8057400250)] was added to the supernatants samples, and then, boiled for 5 minutes followed by size fractionation on SDS–PAGE. Following SDS-PAGE, proteins were transferred to nitrocellulose membranes (GE Healthcare Life Sciences catalog #10600002), which were then blocked for 1 hour with BLOTTO [4% w/v nonfat dry milk/ 0.1% v/v Tween-20 in Tris-buffered saline (TBS: 50 mM Tris, pH 7.5, 150 mM NaCl)] followed by 2 hours or overnight incubation with primary antibodies. After 3 washes with BLOTTO, the membranes were incubated with the appropriate HRP-conjugated secondary antibody for 1 hour. After 3 washes for 10 minutes each with 0.1% v/v Tween-20/TBS, immunoblots were visualized by Pierce ECL Western Blotting Substrate (Thermo Fisher Scientific catalog #34080). The images were acquired with a Mini HD9 imager (Uvitec Ltd., Cambridge, UK) and quantified using the Nine-Alliance software (Uvitec Ltd.).

2.4 | Plasmids

The EGFP-KCTD5 plasmid was previously generated by subcloning the human KCTD5 (hKCTD5) cDNA into the pEGFP-N1 plasmid as described.[20] The hKCTD5 cDNA was obtained from the pKoz Max-HA-KCTD5 plasmid, a kind gift from Dr Steve Goldstein. For Biomolecular fluorescence complementation (BiFC), human TRPM4 (hTRPM4) was

subcloned into the pBiFC-VN155 (I152L) (myc-TRPM4-VN) and pBiFC-VC155 (HA-TRPM4-VC) vectors (provided by Dr Chang-Deng Hu, *via* Addgene plasmids #27097 and #22011, respectively).[22,23] hKCTD5 was subcloned into the pBiFC-VC155 vector (HA-KCTD5-VC). All these constructs were generated using the Gibson Assembly protocol.[24] Ectodomain hemagglutinin (HA)-tagged TRPM4 (FLAG-TRPM4-HA) was inserted into the TRPM4 coding sequence of FLAG-TRPM4 using the pcDNA4/TO-FLAG-TRPM4 vector as template (a kind gift of Dr Pierre Launay) by PCR-based site-directed mutagenesis using the Quickchange site-directed mutagenesis kit (Agilent, Santa Clara, CA, USA, catalog #200518). The HA tag was inserted after Leu 722 residue in the extracellular loop between the S1 and S2 transmembrane segments using the primers: 5′-TAC CCA TAC GAT GTT CCA GAT TAC GCT GAG TTT GAC ATG GAT AGT ATT AAT GGG-3′ and 5′-AGC GTA ATC TGG AAC ATC GTA TGG GTA TAG CTC CTC CCG TGT GGG CTCT CTC TTC TGA-3′. All constructs were verified by DNA sequencing. Plasmids pCI-His-hUbi (His_6-ubiquitin; Addgene plasmid #31815)[25] and BFP-SEC61β (Addgene plasmid #49154)[26] were provided by Drs. Astar Winoto and Gia Voeltz, respectively. Plasmids encoding for shRNAs against KCTD5 were purchased from OriGene, Rockville, MD, USA (catalog #TG303786).

2.5 | Antibodies

Antibodies used for immunofluorescence, immunoblot, immunoprecipitation, proximity ligation assays and immunohistochemistry experiments are listed on Table 1.

2.6 | Immunoprecipitation assay

HEK293 and MCF7 cells were lysed in lysis buffer (50 mM Tris-HCl, 150 mM NaCl, 1 mM EDTA, 1 mM sodium orthovanadate, 5 mM NaF, 1% v/v Triton X-100, pH 7.4) containing as protease inhibitors 1 mM PMSF, and PIC. The lysates were centrifuged at 12 000*g* at 4°C for 10 minutes. The supernatants were incubated with rabbit pAb anti-FLAG (Sigma-Aldrich catalog #F7425) or mAb anti-KCTD5 (Origene catalog # TA501035) antibodies for 16 hours at 4ºC. Immunocomplexes were recovered by the incubation with 30 µL of protein G beads (GE Healthcare Life Sciences catalog #17061802) for 1 hour on a tube rotator at 4°C. After incubation, the beads were washed six times in wash buffer (150 mM NaCl, 1 mM EDTA, 1% v/v Triton X-100, 50 mM Tris-HCl, pH 7.4). Immunocomplexes were eluted by boiling the samples in Reducing Sample Buffer (RSB) for 5 minutes followed by size fractionation on SDS-PAGE.

2.7 | In gel digestion and MS analysis

Mass spectrometry analyses were performed as described.[4] Immunopurified complexes were separated in 12% SDS-PAGE and the bands were excised, diced, and washed twice in 50% v/v acetonitrile (ACN)/25 mM ammonium bicarbonate (Sigma-Aldrich catalogs #270717 and #09830, respectively) and dried 10 minutes in a speed vacuum concentrator. Then, Cys residues were reduced by incubation of the gel pieces in 10 mM dithiothreitol (DTT; Sigma-Aldrich catalog #150460) at 56°C for 1 hour and protected by alkylation by incubating with 55 mM iodoacetamide (Sigma-Aldrich catalog #I6709) at room temperature for 45 minutes in the dark. Gel pieces were then washed 10 minutes in 50 mM ammonium bicarbonate, dehydrated in 50% v/v ACN/50 mM ammonium bicarbonate for 10 minutes and dried in a vacuum concentrator. Dried gel pieces were rehydrated with 100 µL of 50 mM ammonium bicarbonate on ice for 10 minutes, and then, the solution was removed and the gel pieces were covered with 50 mM ammonium bicarbonate containing 10 ng/µL mass spectrometry grade trypsin (Promega, Valencia, CA, USA, catalog # V5280) and incubated overnight at 37°C. Digested peptide mixtures were extracted by vortexing with 50% v/v ACN/5% v/v formic acid for 30 minutes, and completely dried until further analysis. LC-MS/MS procedures were performed at the UC Davis Proteomics Facility using an ultra-performance liquid chromatography (UPLC) system (nanoACQUITY, Waters, Milford, MA, USA) coupled with an ion trap mass spectrometer (LTQ-FT, Finnigan, San Jose, CA, USA) for LC- MS/MS data acquisition. MS/MS spectra were interpreted through the Mascot searches (Matrix Science) with a mass tolerance of 20 ppm, MS/MS tolerance of 0.4 or 0.6 Da, and one missing cleavage site allowed. Carbamidomethylation of cysteine, oxidation of methionine, and phosphorylation on serine, threonine, and tyrosine residues was allowed.

2.8 | Immunofluorescence staining

Forty-eight hours posttransfection, cells were fixed for 15 minutes at 4°C in fixative solution [4% w/v formaldehyde (freshly prepared from paraformaldehyde, Sigma-Aldrich catalog #158127), 4% w/v sucrose (Sigma-Aldrich catalog #S0389) in Dulbecco's phosphate buffered saline (DPBS), pH 7.4]. For surface staining experiments, cells were blocked with blocking solution containing 4% w/v nonfat dry milk in DPBS, for 30 minutes at room temperature and incubated with the anti-HA primary antibody (Table 1) for 4 hours at 4°C. Cells were then permeabilized and blocked with blocking solution containing 0.1%

TABLE 1 List of antibodies

Antibody	Isotype	Dilution	Final [ ], µg/mL	Source	Type	Catalog#	RRID	Purification
Mouse anti-TRPM4	IgG1	1:1000 (IB)	1.5	Origene	mAb	TA500381	AB_2208624	Asc
Mouse anti-TRPM4	IgG1	1:100 (IF)	15	Origene	mAb	TA500381	AB_2208624	Asc
Mouse anti-TRPM4	IgG1	1:50 (IHC)	30	Origene	mAb	TA500381	AB_2208624	Asc
Mouse anti-KCTD5	IgG2b	1:1000 (IB)	1	Origene	mAb	TA501035	AB_11140321	Asc
Mouse anti-KCTD5	IgG2b	(IP)	5	Origene	mAb	TA501035	AB_11140321	Asc
Mouse anti-tubulin	IgG1	1:5000 (IB)	1	Sigma-Aldrich	mAb	T5168	AB_477579	Asc
Rabbit anti-Flag	IgG	(IP)	3	Sigma-Aldrich	pAb	F7425	AB_439687	AP
Mouse anti-HA	IgG2b	1:50 (IF)	5	Roche	mAb	11 583 816 001	AB_514505	AP
Mouse anti-Myc	IgG1	1:100 (PLA)	20	Sigma-Aldrich	mAb	M4439	AB_439694	AP
Mouse anti-EGFP	IgG2a	TC Supernatant	–	NeuroMab	mAb	75-132	AB_10672529	AP
Mouse anti-Ubiquitin	IgG1	1:1000 (IB)	–	Cytoskeleton, Inc	mAb	AUB01	–	Asc
Rabbit anti-KCTD5	IgG	1:100 (PLA)	4.2	Abcam	mAb	Ab194825	–	AP
Rabbit anti-KCTD5	IgG	1:100 (IHC)	4.2	Abcam	mAb	Ab194825	–	AP
Rabbit anti-actin	IgG	1:500 (IB)	1	Cytoskeleton, Inc	pAb	AAN01	AB_10708070	AP
Alexa Fluor 488 conjugated goat anti-Mouse IgG2a	IgG	1:1000	2	Thermo Fisher Scientific	pAb	A-21131	AB_2535771	AP
Alexa Fluor 555 conjugated goat anti-Mouse IgG1	IgG	1:1000	1	Thermo Fisher Scientific	pAb	A-21127	AB_2535769	AP
Alexa Fluor 647 conjugated goat anti-Mouse IgG2b	IgG	1:1000	1	Thermo Fisher Scientific	pAb	A-21241	AB_2535810	AP

Abbreviations: AP, affinity purified; Asc, purified from mouse ascites fluids by affinity chromatography; IB, immunoblot; IF, immunofluorescence; IHC, immunohistochemistry; mAb, monoclonal antibody; pAb, polyclonal antibody; PC, purified from chicken gizzard smooth muscle; PLA, proximity ligation assay.

v/v Triton X-100, 4% w/v nonfat dry milk in DPBS, for 30 minutes at room temperature and incubated with the respective primary antibody (Table 1) for 1 hour at room temperature. After three washes for 10 minutes each, primary antibodies were detected by incubation for 1 hour at room temperature with Alexa-labeled isotype-specific secondary antibodies (Table 1) and Hoechst 33 258 nuclear stain at 200 ng/mL (Thermo Fisher Scientific catalog #H3569). Samples were washed 3 times for 10 minutes each on 0.1% v/v Triton X-100/DPBS and mounted with ProLong Gold (Thermo Fisher Scientific catalog #P36930). Images were acquired with a CCD camera installed on a Carl Zeiss LSM800 microscope with 63X, 1.4 numerical aperture objectives coupled to ZEN software (Carl Zeiss, Oberkochen, Germany).

2.9 | Proximity ligation assay

The assays were carried out using the Duolink in Situ Red Starter Kit Mouse/Rabbit (Sigma-Aldrich catalog #DUO92101) following the manufacturer's instructions. Cells were fixed and permeabilized as described in the previous section, followed by incubation for 1 hour at 37°C in blocking solution. All subsequent incubations were performed in a humid chamber. Mouse anti-TRPM4 mAb and rabbit anti-KCTD5 mAb primary antibodies were added and samples incubated for 1 hour at room temperature. After three washes for 10 minutes each, the samples were incubated with secondary antibodies coupled with oligonucleotides for 1 hour at 37°C. After three washes, ligation solution was added and the samples incubated for 30 minutes at 37°C, followed by a 100 minutes incubation with Ligation Solution at 37°C. The samples were mounted and images were acquired by confocal microscopy. Fluorescence intensity was quantified using the Fiji/Image J software and expressed as fluorescence intensity per cell as described.[27] The acquisition settings were identical for all of the images.

2.10 | Biomolecular fluorescence complementation (BiFC)

BiFC assays were performed as described.[22,23] HEK293 cells were cotransfected with HA-KCTD5-VC and myc-TRPM4-VN. Combination of HA-TRPM4-VC and myc-TRPM4-VN was used as positive control. Then, the cells were fixed and permeabilized as described in the previous sections. Images were acquired by confocal microscopy and the Venus fluorescence intensity was quantified using the Fiji/Image J software and expressed as fluorescence intensity per cell.

2.11 | Computational modeling of the TRPM4-KCTD5 association

To evaluate the molecular assembly between the human TRPM4 channel and the KCTD5 protein, the lowest resolution cryo-EM structure of TRPM4 (PDB ID: 6BCO)[28] and the N-terminal BTB domain of KCTD5 (PDB ID: 3DRZ)[17] were used. Evolutionary Couplings (EC) analyses employing the EV complex server were initially performed to identify putative protein-protein interaction sites.[29] Predicted inter-protein EC pairs with an EVcomplex score >0.1 were used as input restraints for protein-protein docking calculations. Due to the difficulty of evaluating the association of multimeric protein complexes, a first docking approach was performed with HADDOCK v 2.2[30] using only one monomer of both TRPM4 and KCTD5. Based on the predicted inter-ECs, residues 115, 172, 187, 188, 217, 272, 280, 308, 363 in TRPM4 and 46, 59, 60, 70, 94, 99, 107 in KCTD5 were defined as active for docking. The best HADDOCK score conformation was then used as starting point to simulate the interaction between the tetrameric structure of TRPM4 and the pentameric structure of KCTD5 using the Monte Carlo based multi-scale docking algorithm implemented in ROSETTA.[31] Ten thousand docking conformations were generated and clustered using a root-mean-square deviation (RMSD) cutoff value of 5 Å. The structures with the lowest ROSETTA score in each cluster were chosen as representative and structurally analyzed using PyMOL v 1.8.4 (Schrödinger, LLC).

2.12 | Electrophysiological solutions

Intracellular: 140 mM CsCl, 5 mM NaCl, 1 mM $MgCl_2$, 10 mM HEPES, pH 7.2 adjusted with CsOH, and the free Ca^{2+} (10 nM to 1 mM) was calculated with Winmaxc 2.4 software (http://www.stanford.edu/~cpatton/maxc.html). Extracellular: 140 mM NaCl, 5 mM CsCl, 1 mM $MgCl_2$, 1 mM $CaCl_2$, 10 mM HEPES, and 10 mM glucose, adjusted to pH 7.4 with NaOH.

2.13 | Patch clamp recording

TRPM4 currents were recorded using the patch clamp technique in whole cell configuration with an EPC-7 amplifier (HEKA, Holliston, MA, USA). Data were digitized at 10 kHz with a Digidata 1322A (Axon Instruments, San Jose, CA, USA) and low-pass filtered at 1 kHz (Frequency Devices, Ottawa, IL, USA). The step protocols consisted of a 400 ms step at −100 mV from a holding of 0 mV, followed by a 400 ms step at +100 mV and a 800 ms ramp

protocol from −60 to +120 mV. pClamp 9.2 software (Molecular Devices Corp., San Jose, CA, USA) was used for data acquisition and analysis. Patch electrodes (~3 MΩ resistance) were pulled from borosilicate glass (Warner Instruments, Hamden, CT, USA) using a BB-CH puller (Mecanex SA, Geneva, CH). All experiments were conducted at 22 ± 2°C. The time course for current deactivation was fitted to a single exponential equation where τ_{close} represents the time constant for the closing of the channels. The time course for current activation was fitted to a double exponential plus a constant term equation. The expression used was:

$$I = A_1 e^{-t/\tau_{Open1}} + A_2 e^{-t/\tau_{Open2}} + C$$

where A_1 and A_2 correspond to the fractional amplitude for each component and C correspond to maximal current. τ_{Open1} and τ_{Open2} represents the slow and fast time constants, respectively.

The data showing the current dependence on intracellular calcium was fitted to a sigmoidal dose-response curve of the form:

$$I = I_{min} + \frac{I_{max} - I_{min}}{1 + 10^{Log}(EC_{50}) - [Ca^{2+}]_i}$$

2.14 | Ni^{2+}-NTA affinity chromatography

Transfected HEK293 cells were lysed in lysis buffer [0.5% v/v NP-40 (Sigma-Aldrich catalog #I8896), 300 mM NaCl (Merck catalog #1064045000), 50 mM Tris-HCl, pH 8.0, 5 mM NaF, 40 mM Imidazole (Sigma-Aldrich catalog #I202), 1 mM PMSF, and PIC]. The lysates were centrifuged at 12 000*g* at 4°C for 10 minutes. The supernatants were incubated with 70 µL of Ni Sepharose 6 Fast Flow histidine-tagged protein purification resin (GE Healthcare Life Sciences catalog #17531801) for 2 hours on a tube rotator at 4°C. After incubation, the resin was washed ten times in wash buffer (0.5% v/v NP-40, 300 mM NaCl, 50 mM Tris-HCl, pH 8.0, 5 mM NaF, 40 mM Imidazole) for 5 minutes. The retained proteins were eluted by boiling the samples in RSB for 5 minutes, and then, size-fractionated on SDS-PAGE.

2.15 | Surface biotinylation assay

Biotinylation assays were performed as described.[32,33] The cells were grown to 80%-90% confluence on poly-L-lysine (200 µg/mL) treated 35 mm tissue culture dishes. The cells were washed twice with ice-cold DPBS (pH 8.0) and incubated with 500 µg/mL EZ-link sulfo-NHS-LC-biotin (Thermo Fisher Scientific catalog #21335) dissolved in DPBS (pH 8.0) for 30 minutes at room temperature. The reaction was terminated with blocking solution (50 mM Tris, 154 mM NaCl, pH 8.0) and the cells washed twice with ice-cold PBS. The cells labeled with sulfo-NHS-biotin were lysed as described above, and lysates were incubated with streptavidin-agarose (Thermo Fisher Scientific catalog #20351) overnight at 4ºC. The precipitated proteins were eluted with RSB and resolved in SDS-PAGE for further immunoblot analysis.

2.16 | Boyden chamber transwell invasion assays

MEF cells (5.0×10^4 cells) transfected with the plasmids expressing EGFP and EGFP-KCTD5 were plated into 8 µm pore-Transwell chambers (Sigma-Aldrich catalog #CLS3422). Cell migration were induced by adding 10% v/v FBS in the lower chamber for 16 hours at 37°C. The nonmigrating cells were removed and the migrating cells were fixed and stained with 0.2% w/v crystal violet dissolved in 10% v/v ethanol. The migrating cells were counted and expressed as percentage of control.

2.17 | Zebrafish experiments

Zebrafish embryos were obtained by natural spawning and raised at 28°C in E3 medium. Lines used were wild type TU and *Tg(sox17:GFP)*.[34] The Bioethics Committee of the Faculty of Medicine, Universidad de Chile approved animal manipulation protocols. Embryos were injected at the one cell stage using standard procedures with an antisense morpholino against KCTD5 (9 ng/embryo; 5´-CTCTTCTCCGCCATCCCTCCTCT-3´, tagged with lissamine at the 3′ extreme or a standard control morpholino (9 ng/embryo; 5′-AGCTATGACCCCCTCTCAAAATGGC-3′) (Gene Tools LLC., Philomath, OR, USA). Morpholino-dependent KCTD5 silencing was determined by immunoblot. To do that, a pool of embryos obtained from five mates were fractionated in two batches of two hundred embryos. Each batch was injected at the one cell stage with 9 ng of the antisense morpholino against KCTD5 or with 9 ng of a standard control morpholino for control embryos. Embryos were manually dechorianted, anesthetized at 24 hours postfertilization (hpf), and the yolk sac was removed mechanically using a glass Pasteur pipet in cold E3 medium. Twenty deyolked embryos were homogenized in RIPA lysis buffer, supplemented with protease and phosphatase inhibitors, using a microfuge pestle until uniform consistency and incubated for 30 minutes on ice. Lysed samples were centrifugated and the supernatant was analyzed by immunoblot. Whole-mount in situ hybridization was performed as described previously[35] using an antisense Digoxygenin-labeled riboprobe against *tbxta*.[36] Epiboly progression, convergence width, and extension length were measured manually using the Fiji/ImageJ

open software from images obtained using a Nikon SMZ100 stereoscope coupled to a Nikon digital camera. *Tg(sox17:GFP)* line was used for paraxial endoderm cell tracking. Embryos were imaged from shield stage onwards in a LEICA TCS LSI confocal microscope using a 5X objective. Paraxial endoderm cells were tracked manually using the MTrackJ plugin of the Fiji/ImageJ open software. Kinetics parameters were extracted from these tracks.

2.18 | Tissue mRNA expression

The expression of TRPM4 and KCTD5 mRNA in breast cancer was analyzed using OriGene TissueScan Breast Cancer cDNA Array II (OriGene catalog #BCRT102, lot #TH25). The array contains cDNA obtained from 48 clinical samples: 5 normal and 43 breast cancer tissues covering all different disease stages. All of the samples have a pathology report and relevant clinical information publicly available at the manufacturer's website. Amplification of TRPM4, KCTD5, and β-actin cDNAs was carried out using the following primers (Forward/Reverse): TRPM4 (5′-AGAGTGAACTCTTTCGGGGG-3′/5′-TCCATGAGGGAAGCTTCGAG-3′) 250 nM; KCTD5 (5′-GGAGCTGCTGGGATTCCTTT-3′/5′-GTCAGTCTGCACAGTACCCC-3′) 400 nM; β-actin (5′-TGACGTGGACATCCGCAAAG-3′/5′-CTGGAAGGTGGACAGCGAGG-3′) 250 nM. PCR reactions were prepared using SensiMix SYBR Hi-ROX Kit (Bioline, London, UK catalog QT605-05) following manufacturer's instructions and reaction detection was performed using the StepOne Real-Time PCR System (Applied Biosystems, Foster City, CA, USA), using the following cycling conditions: 95°C for 10 minutes, followed by 40 cycles of 95°C for 15 seconds and 60°C for 1 minute, followed by a melt curve starting at 60°C, gradually increasing the temperature by 0.3°C to 95°C. StepOne Software v 2.3 was used for curve analyses. Relative expression was normalized to β-actin and determined using the double delta Ct method.[21]

2.19 | Breast cancer samples immunohistochemistry

Immunohistochemistry studies were performed on formalin-fixed paraffin embedded (FFPE) triple negative breast cancer and normal tissues for TRPM4 and KCTD5 immunodetection. Antigen retrieval was performed by incubating the tissue samples with 0.05% w/v trypsin at 37°C for 20 minutes, and then, at room temperature for 10 minutes. The slides were then treated with 3% v/v hydrogen peroxide solution for 20 minutes and blocked with 10% v/v calf serum, 0.3% v/v Triton X-100 diluted in PBS for 2 hours. The samples were then incubated with a 1:100 dilution of mouse anti-TRPM4 mAb or rabbit anti-KCTD5 mAb antibodies overnight at 4°C. For negative control sections, primary antibody was replaced by nonimmune calf serum. After three washes for 10 minutes each, primary antibodies were detected by incubation in anti-mouse/rabbit IgG RTU biotinylated secondary antibody (Vector Laboratories, Burlingame, CA, USA, catalog #BP-1400) for 30 minutes at room temperature. Secondary antibody labeling was amplified using the ABC Peroxidase Standard Staining Kit (Thermo Scientific catalog #32020) for 30 minutes at room temperature. After three washes with PBS, the immunolabeling signal was detected with DAB Peroxidase substrate (Vector Laboratories catalog #SK-4100). After immunohistochemical procedures, Mayer's hemalum solution (Merck catalog #109249) was used for nuclear counterstaining. Images were acquired with a Leica DFC425C camera installed on a Leica DM2500 CCD microscope with 10X and 40X objectives (Leica, Wetzlar, Germany).

3 | RESULTS

3.1 | KCTD5 is a novel TRPM4-associated protein

As we previously reported,[4] we undertook a mass spectrometry-based proteomics approach to identify TRPM4-associated proteins. We immunopurified FLAG-tagged human TRPM4 from HEK293 cells, and identified as novel candidate interacting proteins 124 copurifying endogenous HEK293 cell proteins with a Mascot score >50.[4] In addition to the numerous FA proteins that we previously reported,[4] the potassium channel tetramerization domain 5 (KCTD5) protein was also a prominent component of this analysis (Mascot Score: 270, Queries matched: 11 peptides), as underscored by the 46% overall sequence coverage obtained (Figure 1A). We validated this interaction by coimmunoprecipitation of coexpressed FLAG-TRPM4 and EGFP-KCTD5 proteins in HEK293 cells (Figure 1B). Moreover, Proximity Ligation Assay (PLA) experiments, which yield a signal from proteins in close proximity to one another[37] generated a positive signal from coexpressed TRPM4 and KCTD5 results (Figure 1C,D). In addition, we performed BiFC assays using TRPM4 and KCTD5 fused to N- and C-terminal half of Venus fluorescent protein, respectively (ie, myc-TRPM4-VN and HA-KCTD5-VC) (Figure 1E-G). We observed that coexpression of these constructs complemented Venus fluorescence in a similar manner as myc-TRPM4-VN and HA-TRPM4-VC (Figure 1F,G). We also found that myc-TRPM4-VN and HA-KCTD5-VC BiFC signal localizes preferentially at the plasma membrane (Figure S1).

Finally, the association of TRPM4 and KCTD5 was evaluated at the molecular level by taking advantage of the currently

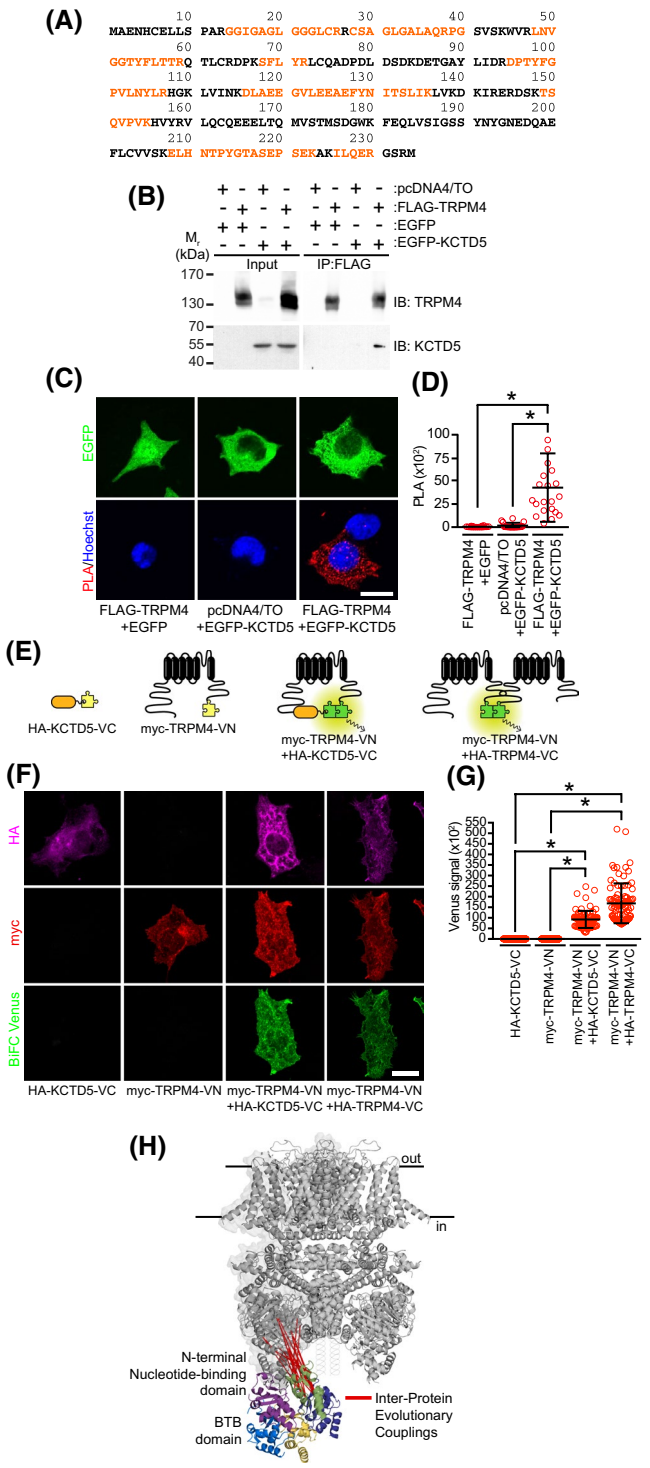

FIGURE 1 TRPM4 interacts with KCTD5. A, Absolute coverage for the KCTD5 protein obtained from immunoprecipitation of TRPM4 and subsequent LC-MS/MS analyses. B, Representative immunoblots of immunoprecipitation products showing the interaction between FLAG-TRPM4 and EGFP-KCTD5 in HEK293 cells. Representative images of results obtained from three independent experiments are shown. C, Representative images of Proximity Ligation Assay (PLA) labeled HEK293 cells expressing the indicated plasmids using mouse anti-TRPM4 mAb and rabbit anti-KCTD5 mAb. PLA positive signal is showed in red. Representative images of results obtained from three independent experiments are shown. Scale Bar: 20 μm. D, Graph shows the mean ± standard deviation (SD) of the PLA signal intensity for TRPM4-KCTD5 interaction per cell from 16, 18, and 21 cells for FLAG-TRPM4+EGFP, pcDNA4/TO+EGFP-KCTD5, and FLAG-TRPM4+EGFP-KCTD5, respectively. Statistical analysis was performed using a one-way ANOVA test, followed by Tukey's multiple comparisons test (*$P < .0001$). E, Cartoon representing the TRPM4 and KCTD5 constructs and combinations used in the BiFC assays. F, Representative images of BiFC assays from HEK293 cells expressing the indicated plasmids. Representative images of results obtained from three independent experiments are shown. Scale Bar: 20 μm. G, Graph shows the mean ± standard deviation (SD) of the Venus fluorescence signal intensity for TRPM4-KCTD5 and TRPM4-TRPM4 (as control) interaction per cell from 94, 91, 88, and 90 cells for HA-KCTD5-VC, myc-TRPM4-VN, HA-KCTD5-VC+myc-TRPM4-VN and HA-TRPM4-VC+myc-TRPM4-VN. Statistical analysis was performed using a one-way ANOVA test, followed by Tukey's multiple comparisons test (*$P < .0001$). H, Lowest score protein-protein docking conformation of TRPM4 (gray) interacting with the BTB domains of KCTD5 pentamer (cartoon in colors). Inter-protein EC predictions (red lines) were used as input restraint for docking

available structures of TRPM4 and KCTD5 proteins.[17,28] Inter-protein contacts predictions obtained by evolutionary couplings (EC) analysis[29] identified residues 115, 172, 187, 188, 217, 272, 280, 308, 363 in the N-terminal nucleotide-binding domain (NBD) of TRPM4 interacting with at least one subunit of the BTB domain of KCTD5 (ie, residues 46, 59, 60, 70, 94, 99, 107). Moreover, protein-protein docking simulations using EC pairs as input restraints revealed the formation of the protein complex assembly (Figure 1H). These data suggest that KCTD5 is a novel interaction partner of the TRPM4 ion channel.

3.2 | KCTD5 regulates TRPM4 channel Ca^{2+} sensitivity

We next determined the role of KCTD5 in regulating TRPM4 activity. We performed whole cell voltage clamp recordings from HEK293 cells expressing TRPM4 and shRNAs against KCTD5 to knockdown endogenous KCTD5 expression, which we verified in immunoblot analyses (Figure 2A). We used 10 μM free intracellular Ca^{2+} or $[Ca^{2+}]_i$ in our recordings to ensure maximal open probability of the TRPM4 channels.[38] We found that shRNA-mediated KCTD5 knockdown diminished TRPM4-mediated currents by ≈50% relative to the scrambled shRNA control (Figure 2B,C). Similar results were obtained from recordings performed in HEK293$^{kctd5-/-}$ cells (Figures S2 and 2D-F). Moreover, we observed that the rescue of the expression of KCTD5 recovers TRPM4 current levels (Figure 2D-F). Cell surface biotinylation labeling experiments revealed that knockdown of KCTD5 did not significantly alter TRPM4 surface expression (Figure 2G,H). Complementary immunofluorescence experiments yielded a consistent picture, such that no differences were observed in the cell surface labeling intensity of external HA-tagged

TRPM4 in intact HEK293 cells expressing shRNA^{Scramble} and shRNA^{KCTD5} (Figure 2I-K). Together these results support that KCTD5 regulates the activity of TRPM4 channels through a mechanism that does not involve altered TRPM4 surface expression.

We next assessed the effect of KCTD5 overexpression on TRPM4 activity. We did not observe significant differences between TRPM4 currents in cells without and with KCTD5 overexpression at 10 μM $[Ca^{2+}]_i$ (EGFP: 81.96 ± 6.70, n = 8 cells vs EGFP-KCTD5: 90.44 ± 5.12, n = 8 cells). We then performed similar experiments at physiological resting levels of $[Ca^{2+}]_i$ (ie, 100 nM free Ca^{2+}) and found that exogenous EGFP-KCTD5 expression yielded ≈2x increases in whole cell TRPM4 currents (Figure 2L,M). We next evaluated EGFP-KCTD5 coexpression impacted the Ca^{2+} sensitivity of TRPM4 channels (Figure 2N). We found that the Ca^{2+} sensitivity of TRPM4 channels coexpressed with EGFP-KCTD5 increased ≈2x compared to the EGFP control (EC_{50} values of 234.24 ± 59.14 nM and 107.78 ± 57.84 nM for EGFP and EGFP-KCTD5, respectively). This suggests that endogenous levels of KCTD5 in HEK293 cells fully support TRPM4 activity when $[Ca^{2+}]_i$ is elevated, and that overexpression of KCTD5 yields TRPM4 channels that are active at resting levels of $[Ca^{2+}]_i$.

We analyzed the kinetic parameters of the activation and deactivation of TRPM4 currents by fitting a two-exponential equation including a time-independent component to model the activation process, and a single exponential equation to model the deactivation process (see Experimental Procedures). We found that the reduced TRPM4 currents in KCTD5 knockdown cells did not exhibit differences in their activation time constants or fractional amplitude

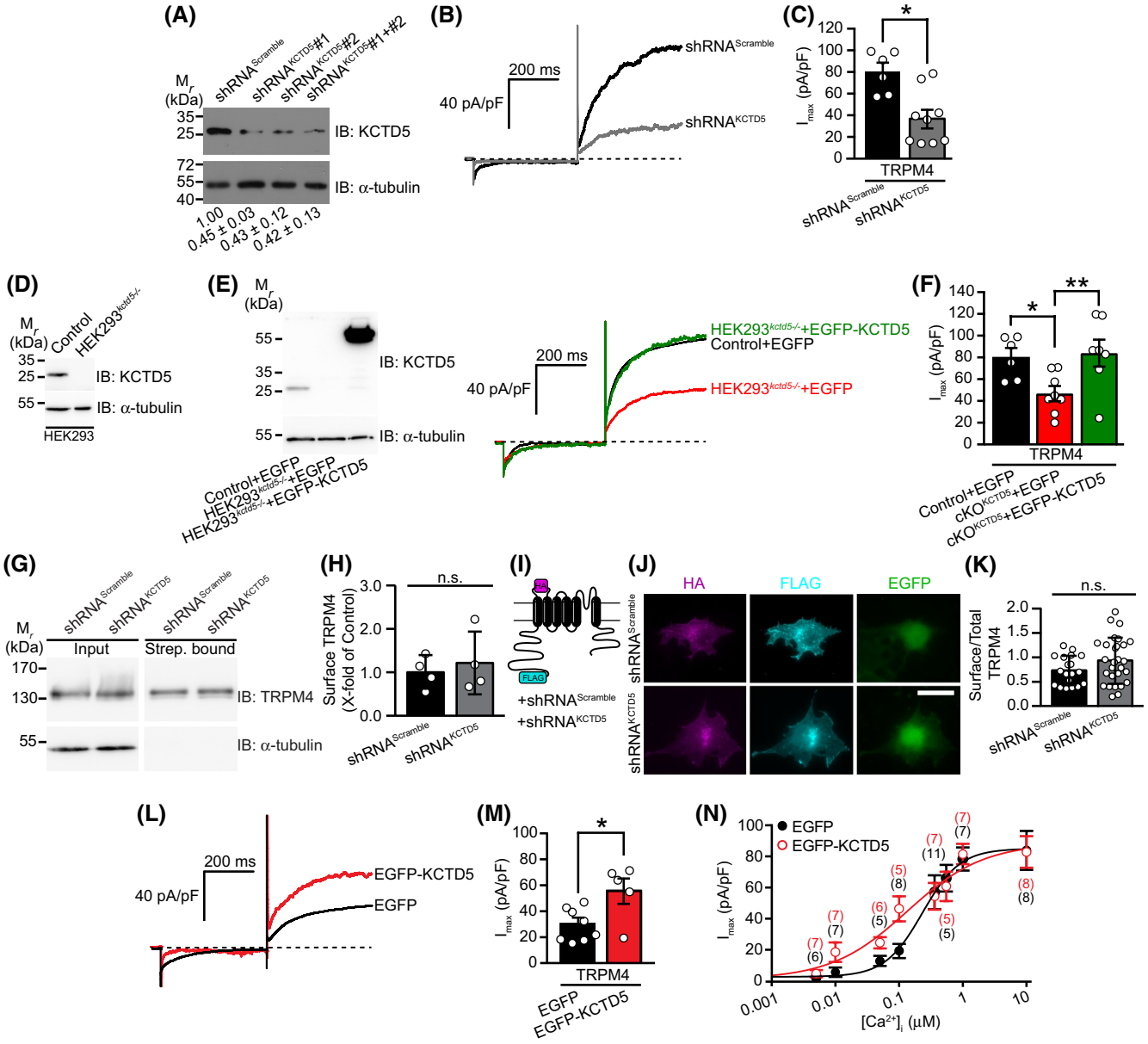

FIGURE 2 KCTD5 regulates TRPM4 activity. A, Representative immunoblot demonstrating shRNA-mediated KCTD5 silencing in HEK293 cells. Numbers below each lane correspond to mean ± SD of the KCTD5 immunoreactive band quantification normalized against $shRNA^{Scramble}$ control. B, Whole cell currents recorded from HEK293 cells expressing FLAG-TRPM4 and either $shRNA^{KCTD5}$ or the $shRNA^{Scramble}$ control. Data correspond to the maximal current recorded at 10 μM $[Ca^{2+}]_i$. C, Graphs depicting the maximal currents [mean ± standard error of the mean (SEM)] obtained at +100 mV recorded at 10 μM $[Ca^{2+}]_i$ from 6 or 9 cells, respectively, from HEK293 cells expressing FLAG-TRPM4 and either the $shRNA^{Scramble}$ control or $shRNA^{KCTD5}$ (unpaired *t* test, $*P = .0034$). D, Representative immunoblot for KCTD5 expression from wild type, CRISPR-mediated KCTD5 knockout ($HEK293^{kctd5-/-}$) and $HEK293^{kctd5-/-}$ +EGFP-KCTD5 cells. E, Whole cell recordings of FLAG-TRPM4 currents expressed in wild type, $HEK293^{kctd5-/-}$ and $HEK293^{kctd5-/-}$ +EGFP-KCTD5 HEK293 cells. Data correspond to the maximal current recorded at 10 μM $[Ca^{2+}]_i$. F, Graphs depicting the maximal currents [mean ± standard error of the mean (SEM)] obtained at +100 mV recorded at 10 μM $[Ca^{2+}]_i$ from 6, 8, and 7 cells, respectively, from control expressing FLAG-TRPM4 (one-way ANOVA test, followed by Tukey's multiple comparisons test ($*P = .0460$, $**P = .0188$). G, Representative immunoblot of cell surface biotinylation assays from COS-7 cells transfected with FLAG-TRPM4 and either $shRNA^{Scramble}$ or $shRNA^{KCTD5}$. Representative images of results obtained from five independent experiments are shown. H, Graph shows the mean ± SD signal intensity of TRPM4 levels in the streptavidin bound fraction (Strept. bound) relative to the input, and normalized against the $shRNA^{Scramble}$ control. Statistical analysis was performed using Mann-Whitney test, n = 5, $P = .1270$ compared to $shRNA^{Scramble}$ control. n.s., no significant. I, Cartoon representing the TRPM4 HA-tagged construct. Transmembrane segments (black segments) and the position of external HA tag (magenta) and cytoplasmic FLAG tag (cyan) are shown. J, Immunocytochemical analysis of external HA-tagged FLAG-TRPM4 channels in intact (magenta) and permeabilized (cyan) COS-7 cells transiently cotransfected with either $shRNA^{Scramble}$ or $shRNA^{KCTD5}$ (green). Scale bar: 20 μm. K, Graph showing the ratio of the HA to FLAG signal intensity ± SD Data were obtained from five independent experiments of 19 and 27 cells for $shRNA^{Scramble}$ and $shRNA^{KCTD5}$ conditions, respectively. Statistical analysis was performed using unpaired *t* test, n = 5, $P = .1259$ compared to $shRNA^{Scramble}$ control. n.s., not significant. L, Whole cell currents recorded from HEK293 cells expressing FLAG-TRPM4 and either EGFP-KCTD5 or EGFP as control. Data correspond to the maximal current recorded at 100 nM $[Ca^{2+}]_i$. M, Graphs depicting the maximal currents [mean ± standard error of the mean (SEM)] obtained at +100 mV from 8 and 5 cells for TRPM4 expressing EGFP and EGFP-KCTD5, respectively (unpaired *t* test, $*P = .0143$). N, Ca^{2+} dose–response relationship for TRPM4 maximal currents in cells coexpressing EGFP-KCTD5 (red circles) or coexpressing EGFP as control (black circles). The Ca^{2+} concentration response data were fitted to a single Hill equation (see Experimental Procedures). n are indicated in black and red for EGFP and EGFP-KCTD5, respectively. Significant differences between curves were determined by using Fischer test ($P = 5.2874 \times 10^{-6}$)

when compared to control cells (Figure S3A). Analyses of TRPM4 currents in cells overexpressing KCTD5 at 100 nM $[Ca^{2+}]_i$ revealed that while KCTD5 overexpression does not change the opening exponential components (Figure S3B), the deactivation kinetics at −100 mV were significantly faster when compared to control cells. These results suggest that KCTD5 is a positive regulator of TRPM4 through a mechanism that also yields alterations in certain channel kinetic properties.

3.3 | KCTD5 does not promote TRPM4 ubiquitination

Since KCTD5 is an ubiquitin E3-ligase adapter,[15] we next determined whether altering KCTD5 expression impacts TRPM4 ubiquitination. We coexpressed TRPM4 and EGFP-KCTD5 and polyhistidine-tagged ubiquitin (His_6-Ub) in HEK293 cells and performed Ni^{2+}-NTA affinity chromatography to purify polyhistidine-containing (ie, ubiquitinated) proteins. Interestingly, we found that TRPM4 is ubiquitinated in both control (EGFP) and EGFP-KCTD5 transfected cells (Figure S4A). Both the immature and mature populations of TRPM4 channels, which can be distinguished by their distinct electrophoretic mobility on SDS gels[39,40] are ubiquitinated (Figure S4A). Overall, we did not observe significant changes in the extent of TRPM4 ubiquitination upon KCTD5 overexpression (Figure S4A,B). Consistently, we also did not detect any overall changes in ubiquitination of TRPM4 protein upon KCTD5 silencing (Figure S4C,D).

3.4 | KCTD5 regulates cell migration and contractility

Since TRPM4 activity regulates cell migration and contractility, we hypothesized that KCTD5 may also impact these processes through the regulation of TRPM4 channel activity defined above. We evaluated the role of KCTD5 in cell migration and contractility by performing Transwell chamber migration and 3D collagen matrix contractility assays. We found that MEF cells expressing exogenous KCTD5 have increased migration (Figure 3A) and contractility (Figure 3B). Also, we found that pharmacological inhibition of TRPM4 with 9-phenanthrol or shRNA-based TRPM4 silencing[4,33] (Figure S5), abolished the KCTD5-dependent effects on cell migration, supporting that these effects were mediated through TRPM4 (Figure 3C,D).

We next assessed the in vivo effects of manipulating KCTD5 expression on cell migration employing an established zebrafish model of cell migration.[41,42] We used morpholino antisense oligonucleotide injection into embryos to silence KCTD5 expression (Figure 4A). We observed significantly delayed epiboly progression, conversion width, and extension length in the KCTD5 morphant embryos in vivo (Figure 4B,C). We found that endodermal cells

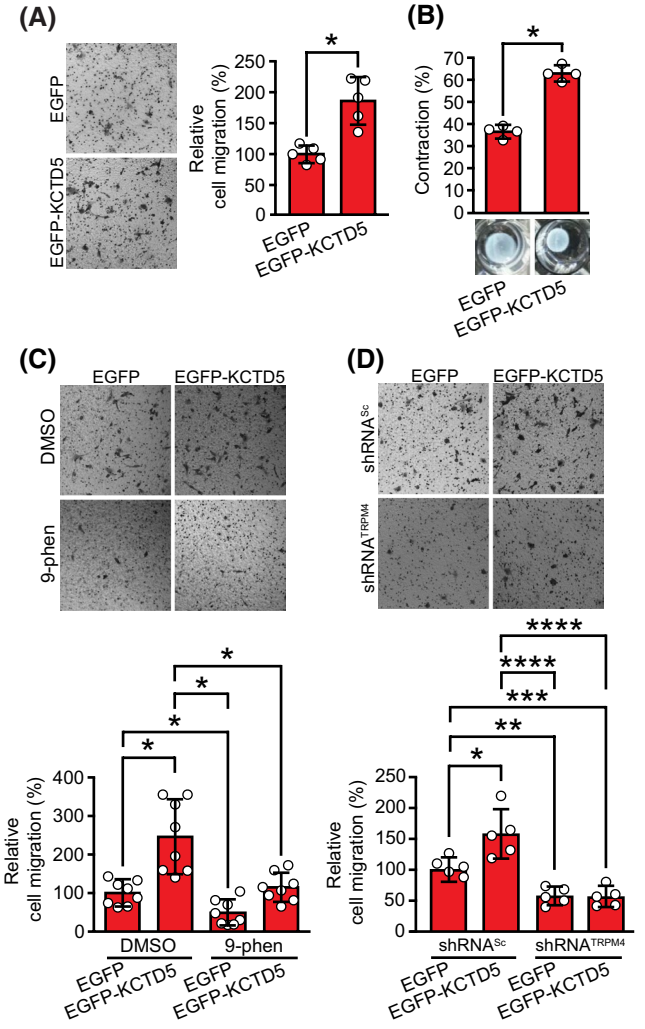

FIGURE 3 KCTD5 regulates cell migration. A, Transwell Boyden chamber migration assays of MEF cells transfected with EGFP or EGFP-KCTD5 for 48 hours, and then, stimulated with 10% v/v serum for 16 hours. Graph shows the percentage (mean ± SD) of cell migration normalized to EGFP-transfected cells. Data were obtained from five independent experiments, and statistical significance was analyzed by a Mann-Whitney test, $*P < .05$ for EGFP-KCTD5 compared to the EGFP control. B, Three-dimensional contraction assay of MEFs transfected with EGFP or EGFP-KCTD5. Contraction was induced by incubating the immersed cells with 10% v/v serum for 48 hours. The upper graph represents the data collected from four independent assays. Statistical analysis was performed using a Mann-Whitney test ($*P < .001$). C, Transwell Boyden chamber migration assays of MEF cells transfected with EGFP or EGFP-KCTD5 for 48 hours, and then, stimulated with 10% v/v serum and treated with DMSO and 10 μM 9-phenanthrol (9-phen) for 16 hours. Graph shows the percentage (mean ± SD) of cell migration normalized to EGFP-transfected cells. Data obtained from eight independent experiments, and statistical significance was analyzed by a one-way ANOVA, followed by Tukey's multiple comparisons test, $*P < .0001$. D, Transwell Boyden chamber migration assays of MEF cells transfected with EGFP or EGFP-KCTD5 and $shRNA^{Scramble}$ ($shRNA^{Sc}$) and $shRNA^{TRPM4}$ for 48 hours, and then, stimulated with 10% v/v serum for 16 hours. Graph shows the percentage (mean ± SD) of cell migration normalized to EGFP-transfected cells. Data obtained from five independent experiments, and statistical significance was analyzed by a one-way ANOVA, followed by Tukey's multiple comparisons test ($*P = .0040$, $**P = .0368$, $***P = .0328$, $****P < .0001$)

in KCTD5 morphant embryos have diminished trajectory and speed (Figure 4D-F), suggesting that diminished cell migration underlies the morphological differences in the oligonucleotide-injected embryos. Together, these results suggest that KCTD5 is a novel regulator of cell migration.

3.5 | Expression of TRPM4 and KCTD5 is increased in breast cancer samples

A series of recent studies demonstrated that TRPM4 expression is increased in several types of cancer.[6,7,10,43] Given our findings that KCTD5 regulates TRPM4 activity and impacts TRPM4-mediated cellular processes, we hypothesized that KCTD5 may also be increased in certain cancers. Interestingly, transcriptomics data in public databases[44] suggest an increased expression of both TRPM4 and KCTD5 genes in breast cancer samples. To begin to investigate KCTD5 in breast cancer, we first used immunoblot assays to evaluate the relative expression of KCTD5 and TRPM4 proteins in four breast cell lines: MCF10A, an epithelial mammary gland cell line, T47D, an estrogen receptor/progesterone receptor positive (ER+/PR+) breast cancer cell line, MCF7, an ER+cell line, and MDA MB-231 and 4T1 cells, models for triple negative breast cancer. We observed that TRPM4 expression is increased in MCF7 and 4T1 cells (Figure 5A,B). A distinct pattern was seen for KCTD5 protein expression, with increased levels in MDA MB-231 and 4T1 cells (Figure 5A,B). As such these breast cancer cells lines overexpress TRPM4, KCTD5 or both. Moreover, we validated TRPM4-KCTD5 endogenous interaction from MCF7 lysates (Figure 5C).

We next used real-time qPCR to evaluate the expression level of TRPM4 and KCTD5 mRNA in normal breast tissue and breast cancer tumors from 48 patients. When averaged across all samples, both TRPM4 and KCTD5 mRNAs are significantly up regulated in breast cancer tumors vs normal breast tissue samples from these 48 breast cancer patients (Figure 5D). We then determined whether the increased mRNA levels of KCTD5 and TRPM4 are related to defined subtypes of breast cancer and/or stages of the disease. We analyzed the mRNA expression data relative to the Nottingham score,[45] TNM classification[46] and biomarker characterization[47] of each of the individual tumor samples from these 48 breast cancer patients. We found that TRPM4 and KCTD5 expression are significantly increased in samples from patients with intermediate (G2) and high-grade (G3) breast

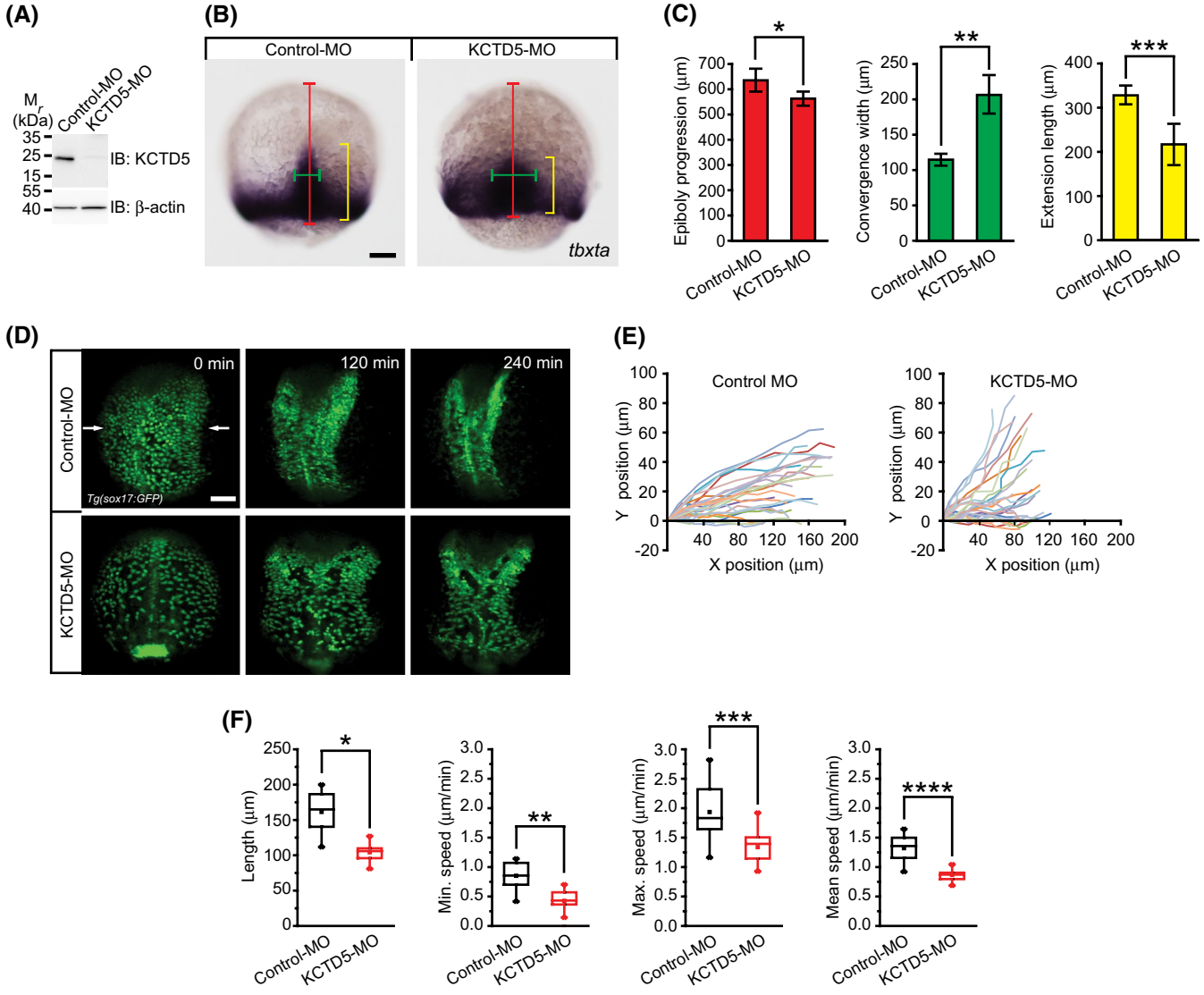

FIGURE 4 Global knockdown of KCTD5 in zebrafish disturbs cell migration during early development. A, Representative immunoblot demonstrating KCTD5-specific antisense morpholino -mediated KCTD5 silencing in zebrafish embryos. B, T-box transcription factor TA (*tbxta*) expression at 75% of epiboly in embryos injected with a control or a KCTD5-specific antisense morpholino. Red, green, and yellow brackets indicate epiboly progression, convergence width, and extension length, respectively. Scale bar: 100 μm. C, Quantification of epiboly progression (red), convergence width (green) and extension length (yellow) from three pattern expressions of *tbxta* in control and KCTD5 morphants (Control-MO, n = 61 embryos; KCTD5-MO, n = 71 embryos). Statistical analysis was performed by using a *t* test (*$P = .0453$, **$P = .0034$, ***$P = .0132$). D, Dorsal views of confocal z-stack maximum projections from 90% epiboly of Tg(*sox17:GFP*) control and KCTD5 morphants used to tracked endodermal cells (green cells). Arrows indicate the migration direction of endodermal cells during their convergence to the embryonic midline. Scale bar: 100 μm. E, Endodermal cell tracking of control (left, n = 24 medial endodermal cells) and KCTD5 morphants (right, n = 26 medial endodermal cells) for 120 minutes from 5 and 4 embryos for Control-MO and KCTD5-MO, respectively. F, Quantification of the trajectory length, minimum speed, maximum speed and mean speed during 120 minutes of endodermal cell migration. Statistical analysis was performed using a *t* test (*$P = 8.5044 \times 10^{-13}$, **$P = 1.9195 \times 10^{-10}$, ***$P = 2.6501 \times 10^{-6}$, ****$P = 9.8280 \times 10^{-11}$)

cancer (Figure 5E) based on the Nottingham Score,[45] which represent breast cancers comprising poorly differentiated and highly proliferative tumor tissue. When we evaluated these data based on the TNM stage classification, related to size of the primary tumor, compromised lymph nodes and the presence of metastasis, we observed significant differences for TRPM4 expression in IIB, IIA, and IV stages (Figure 5F). However, KCTD5 expression increases in I, IIA, and IIIA TNM stages (Figure 5F). When we analyzed the data based on biomarker characterization, we found that both TRPM4 and KCTD5 expression are increased in ER^+/PR^+ and Triple Negative samples (Figure 5G).

Given the increased level of both TRPM4 and KCTD5 transcripts in triple negative breast cancer mRNA samples, we performed immunohistochemistry for both proteins in normal breast and triple negative cancer tissues. Immunolabeling for

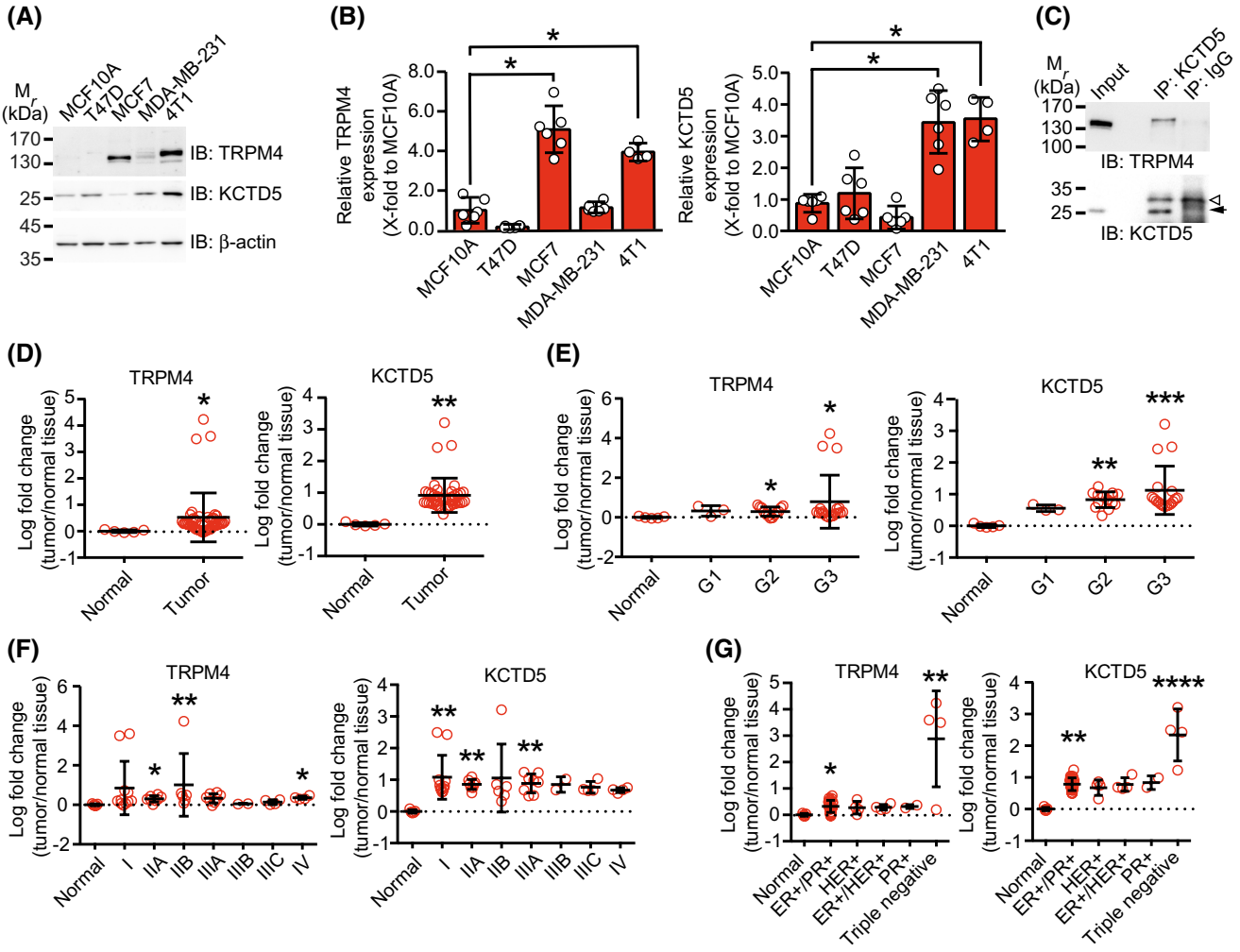

FIGURE 5 TRPM4 and KCTD5 expression are elevated in breast cancer samples. A, Representative immunoblot showing TRPM4 and KCTD5 protein expression from MCF10A, T47D, MCF7, MDA-MB-231, and 4T1 breast cell lines. Representative images of results obtained from five independent experiments are shown. B, Graphs representing data from panel A for TRPM4 and KCTD5 protein expression. The protein levels were normalized to β-actin control and normalized relative to expression in MCF10A cells. Statistical significance was analyzed by a one-way ANOVA, followed by Tukey's multiple comparisons test, $*P < .0001$. C, Representative immunoblots of immunoprecipitation products showing the TRPM4-KCTD5 interaction in MCF-7 cells. Representative images of results obtained from four independent experiments are shown. Arrowhead indicates IgG light chain. Arrow shows KCTD5 immunoreactive band. D-G, Graphs depicting TRPM4 and KCTD5 mRNA expression levels in breast cancer tumors compared (n = 43 samples) to normal tissue (n = 5 samples). The mRNA levels were normalized to β-actin mRNA expression. D, TRPM4 and KCTD5 relative mRNA expression in breast cancer tumors relative to normal tissue. Statistical significance was analyzed by using Mann-Whitney test ($*P < .0006$, $**P < .0001$). E-G, Relative mRNA expression correlated to different tumor classification systems: Nottingham grade (E), TNM classification (F), and biomarker (G). Results are represented as mean ± SD Statistical significance was analyzed by using Kruskal-Wallis test ($*P \leq .05$, $**P \leq .01$, $***P \leq .001$, $****P \leq .0001$ relative to normal tissue expression)

TRPM4 and KCTD5 was not detected in conserved glands of normal appearance (Figure 6A). However, a heterogeneous KCTD5 immunolabeling pattern was observed in areas of high-grade carcinoma, identified by the variability of nuclear shape and increased nuclear size, showing different intensities along the same tumor sample section (Figure 6B). TRPM4 immunolabeling was also heterogeneous across different areas with moderately positive or intense, but heterogeneous TRPM4 signal present in high-grade neoplastic tissue (Figure 6B). Together, these data suggest that the levels of both TRPM4 and KCTD5 are elevated in highly malignant breast cancers with poor prognoses, raising the possibility that their coincident overexpression may act synergistically to enhance TRPM4 activity.

4 | DISCUSSION

Increased TRPM4 activity has been proposed to contribute to the pathophysiology of different cancers[6,7,43,48] as well as other pathological states.[49-54] As such, studies elucidating novel mechanisms of TRPM4 regulation are of interest

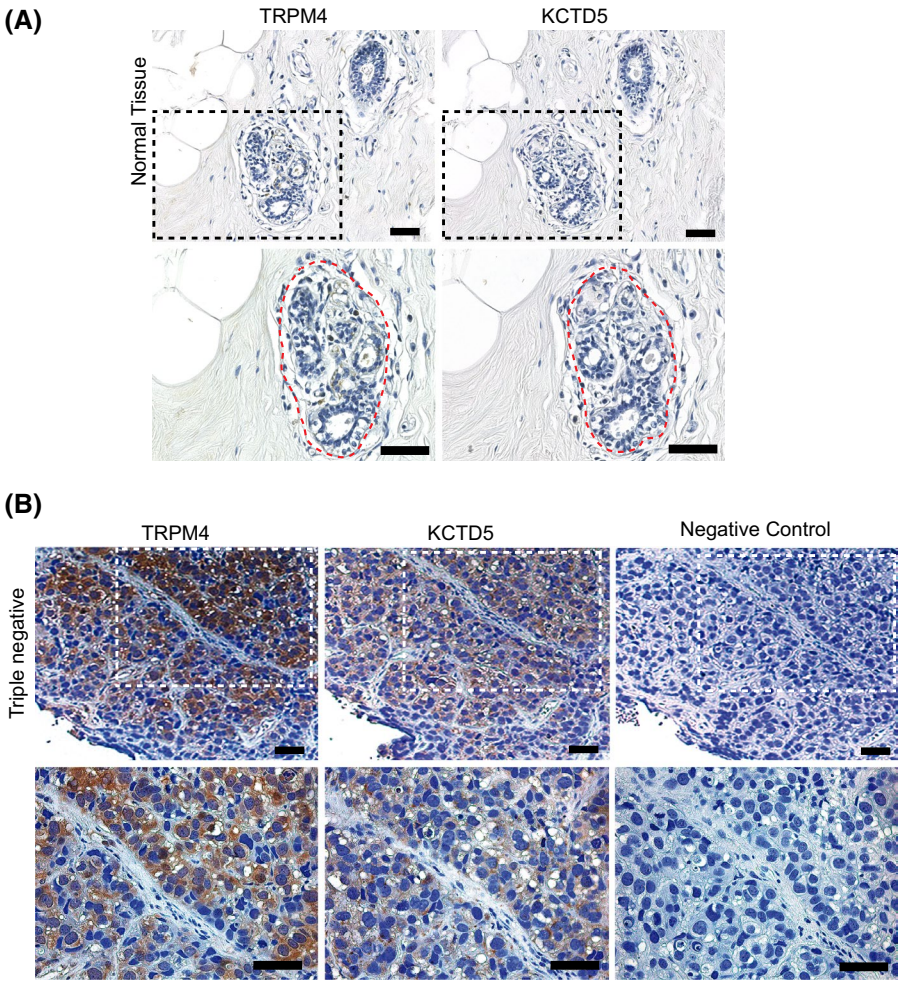

FIGURE 6 Immunohistochemical detection of TRPM4 and KCTD5 expression in normal and triple negative breast cancer tissue. A, Serial sections from normal breast tissue including glands (selected area) in a breast lobule showing negative immunostaining for TRPM4 and KCTD5 proteins. B, Triple negative breast cancer tissue showing positive signal for TRPM4 and KCTD5 in undifferentiated tissue. Note the increased nuclear size and shape heterogeneity of neoplastic cells compared to the normal gland cells nuclei present in panel A. Negative controls of the sections are included in the right-hand panels. Serial sections were used for TRPM4 and KCTD5 staining and negative controls. Lower panels show 40× magnification of the insets. Scale Bar in insets = 50 μm

from a standpoint of both basic and applied biomedical research. Here, we use mass spectrometry-based proteomics to identify to KCTD5 as a novel TRPM4-interacting protein. Moreover, we demonstrate that KCTD5 is a novel positive regulator of TRPM4 channel activity by impacting the biophysical properties of the TRPM4 channels, but not their surface expression. We also find that manipulating KCTD5 expression levels impacts TRPM4-dependent regulation of cell migration, and that both TRPM4 and KCTD5 are upregulated in pathological states. This points to a model whereby TRPM4 activity reflects the combined contributions of TRPM4 itself and the regulatory KCTD5 interacting protein.

Previous studies demonstrated that KCTD5 interacts with Cullin3, an E3 ligase that participates in the process of ubiquitination.[15,16,55] This interaction promotes poly-[16] and mono-ubiquitination[56] of several proteins. Ubiquitination is a well-known negative regulatory mechanism for membrane stability of ion channels, by affecting endocytosis and degradation of these proteins.[57-61] Mass spectrometry-based metaproteomics analyses identified that six lysine residues are candidates for ubiquitination in the TRPM4 protein sequence (ie, di-Gly modified Lys residues).[62,63] Here, we present the first biochemical data supporting that TRPM4 is ubiquitinated. We observed that both immature (ER) and mature (post-ER) forms of TRPM4[39,40] are ubiquitinated, suggesting that TRPM4 ubiquitination begins at an early stage in TRPM4 biosynthesis. This raises the possibility that the ubiquitin ligases involved in this process might regulate TRPM4 biosynthetic maturation, intracellular trafficking, and activity. It is important to note that our results showed that changes in KCTD5 expression do not affect the overall ubiquitination state of TRPM4 protein. However, as our experiments do not distinguish mono- vs poly-ubiquitination

or identify the ubiquitinated sites, it is possible that KCTD5 could impact the pattern of ubiquitination sites, as well as the nature of ubiquitination at those sites.

Our results provide a consistent pattern of KCTD5 acting as a positive regulator of TRPM4 activity. However, KCTD5 appears to exert these effects through the increased activity of plasma membrane TRPM4 channels, and not through increasing the levels of plasma membrane TRPM4 channels. We demonstrated that coexpression with KCTD5 causes a 2-fold increase in Ca^{2+} sensitivity of TRPM4 channels. Moreover, we determined that exogenous KCTD5 causes a significant acceleration of deactivation kinetics. Together, these data suggest that KCTD5 is a novel regulator of the biophysical properties of the channel. Thus, subtle and local changes in Ca^{2+} levels in TRPM4-expressing subcellular compartments, such as at FA complexes, might substantially impact TRPM4 activity through a mechanism impacted by KCTD5 expression levels.

Our data suggest that KCTD5 does not detectably alter the overall ubiquitination state of TRPM4 channels. Thus, it is possible that through its direct interaction with TRPM4, as supported by our co-IP, PLA, and BiFC results, KCTD5 acts to allosterically modulate TRPM4 activity. Consistent with this model, other KCTD proteins regulate the activity of ion channels and receptors in an ubiquitination-independent manner.[64-66] However, we cannot discard an alternative model whereby KCTD5 expression leads to enhanced ubiquitination of TRPM4 at only a small subset of its 39 cytoplasmic lysine residues, such that the overall impact is not substantial enough to be detectable in our ubiquitination assays. It is interesting to note that candidate ubiquitinated lysine residues are found in the highly conserved TRP domain that has been shown to play a key role in allosteric modulation of TRP channel activity,[67,68] and in the putative pleckstrin homology[69] and calmodulin-binding domains that define the Ca^{2+} sensitivity of TRPM4 channels.[28,38] As such, KCTD5-mediated changes in the ubiquitination state of a small number of key residues could impact the gating properties of TRPM4 channels through conformational changes in the TRP domain or by impacting calmodulin binding to impact Ca^{2+} sensitivity, respectively. In addition, there exist other ubiquitin-dependent mechanisms that may contribute to the observed impact of KCTD5 on TRPM4, for example the conditional participation of other substrates for KCTD5-mediated ubiquitination.

Our previous studies have established a role for TRPM4 channel activity in cell migration and FA dynamics.[4] Here, we demonstrate that manipulating KCTD5 expression also impact FAs and cell migration. Our results show that KCTD5 regulates cell migration as well in an in vivo animal model using a morpholino-based silencing strategy.[70] In zebrafish, we found that the abrogation of KCTD5 give raise defects in the migration of endoderm during gastrulation. Thus, our outcomes are consistent in both experimental models. We also showed that the effects of heterologous expression of KCTD5 are abolished by the TRPM4 inhibition and silencing. This supports that the effects of KCTD5 on cell migration are mediated through its interaction with and regulation of TRPM4. This is consistent with our electrophysiological data that show that KCTD5 is a positive modulator of TRPM4 function. Given that TRPM4 activity is crucial in regulating diverse physiological processes,[1,2,4,71-73] the novel KCTD5-mediated mode of TRPM4 regulation that we identified here could help shape physiological regulation of these processes. Further studies using complementary loss-of -function strategies (eg, CRISPR-based knockout models) will allow to confirm these results.

Aberrant KCTD5-mediated regulation of TRPM4 could also play a role in the pathophysiology of numerous diseases that have been linked to a gain-of-function in TRPM4 activity.[49-54,74] In particular, a number of studies have reported elevated expression of TRPM4 in cancer.[6,7,43,48] For instance, TRPM4 promotes cell migration and promotes epithelial to mesenchymal transition of prostate cancer cells,[9] and recent evidence supports using TRPM4 expression as a clinical biomarker for biochemical recurrence in prostate cancer implicated in cell migration and proliferation of malignant cells.[8-10,43,75] Enhanced expression of KCTD protein has been described in medulloblastoma, gastrointestinal, and colon cancer.[76,77] We observed an increased TRPM4 expression in breast cancer tumors. We also provide new information that KCTD5 expression is also increased in breast cancer tumors. Interestingly, our data shows that KCTD5 mRNA levels are increased in poorly differentiated breast cancer subtypes (ie, Nottingham classification).[45] Our findings also suggest that both TRPM4 and KCTD5 expression are increased in the aggressive triple negative subtype, which has the highest mortality rate, poor prognosis, and lacks of specialized treatment.[78,79] Importantly, KCTD5 expression was higher in high-grade tumors with heterogeneous pattern, which exhibit moderate or intense KCTD5 labeling. This is consistent with the diversity of cell subpopulations described for breast cancer.[80,81] Since our data suggest that KCTD5 is a positive regulator of TRPM4 that increases the Ca^{2+} sensitivity of these channels, increased expression of KCTD5 might constitute a key regulator of the malignancy of these types of tumor by potentiating the constitutive activity of TRPM4 and TRPM4-dependent migration, thereby contributing to the tumor aggressiveness of this type of cancer. Given their enhanced and in some cases coordinately increased expression in these forms of breast cancer, TRPM4, and KCTD5 might constitute novel potential biomarkers for

complementary diagnostics for malignancy and progression of breast cancer. Future studies focused on testing whether pharmacologically uncoupling TRPM4-KCTD5 interaction will impact migration, invasiveness and survival of breast cancer tumors may support that TRPM4 and KCTD5 may not only serve as potential diagnostics but also therapeutics targets.

ACKNOWLEDGMENTS

We thank to Mr Aldo Ghisoni, Mr Álvaro Gómez, and Ms Daniela Ibarra for preliminary studies. We are grateful to Mr Nicanor Villarroel for technical assistance. We also thank to Mr Daniel Valdés and Dr Claudio Acuña (Microscopy Core Facility, Universidad de Santiago de Chile) for helpful advice on confocal microscopy acquisition. We thank to Drs. Steve Goldstein, Pierre Launay, Chang-Deng Hu, Astar Winoto, and Gia Voeltz for shared plasmids. Mass spectrometry was performed at the University of California Davis Proteomics Facility. FONDECYT Grant 1160518 (to O.Cerda) funded this work. The Millennium Nucleus of Ion Channel-Associated Diseases (MiNICAD), the Biomedical Neuroscience Institute (P09-015-F) and the Millennium Nucleus on Physics Active Matter are supported by the Iniciativa Científica Milenio of the Ministry of Economy, Development and Tourism (Chile). FONDECYT Grants 11170291, 11170223, 1171155, 1190806, 1160900, and 1181263 funded to F.Jaña, A.Vergara-Jaque, H.Poblete, M.L.Concha, D.Varela, and M.Cáceres, respectively. The Center for Geroscience, Brain Health and Metabolism, GERO (to M.L.Concha) is funded by FONDAP 15150012. I.Silva, M.P. Saldías, P.Cruz, and B.Lavanderos are recipients of Doctoral Fellowship from the Chilean National Council for Sciences and Technology (CONICYT). Confocal microscopy acquisition was performed at the Microscopy Core Facility at Universidad de Santiago de Chile, funded by FONDEQUIP EQM150069.

CONFLICT OF INTEREST

The authors declare no conflict of interests.

AUTHORS CONTRIBUTIONS

O. Cerda designed research. J. Rivas, N. Díaz, I. Silva, D. Morales, M.P. Saldías, E. Pulgar, A. Álvarez, P. Cruz, G. Flores, A. Colombo, C. Blanco, B. Lavanderos, D. Maureira, A. Vergara-Jaque, H. Poblete, M. Cáceres, and O. Cerda performed research. J. Rivas, N. Díaz, I. Silva, D. Morales, M.P. Saldías, E. Pulgar, A. Álvarez, P. Cruz, G. Flores, A. Colombo, C. Blanco, B. Lavanderos, D. Maureira, H.R. Contreras, F. Jaña, I. Gallegos, A. Vergara-Jaque, H. Poblete, W. González, D. Varela, J. S. Trimmer, M. Cáceres, and O. Cerda analyzed data. M.L. Concha provided reagents. J. Rivas, N. Díaz, I. Silva, J. S. Trimmer, and O. Cerda wrote the manuscript.

REFERENCES

1. Launay P, Fleig A, Perraud AL, Scharenberg AM, Penner R, Kinet JP. TRPM4 is a Ca2+-activated nonselective cation channel mediating cell membrane depolarization. *Cell*. 2002;109:397-407.
2. Barbet G, Demion M, Moura IC, et al. The calcium-activated nonselective cation channel TRPM4 is essential for the migration but not the maturation of dendritic cells. *Nat Immunol*. 2008;9:1148-1156.
3. Shimizu T, Owsianik G, Freichel M, Flockerzi V, Nilius B, Vennekens R. TRPM4 regulates migration of mast cells in mice. *Cell Calcium*. 2009;45:226-232.
4. Caceres M, Ortiz L, Recabarren T, et al. TRPM4 is a novel component of the adhesome required for focal adhesion disassembly, migration and contractility. *PLoS One*. 2015;10:e0130540.
5. Weber KS, Hildner K, Murphy KM, Allen PM. Trpm4 differentially regulates Th1 and Th2 function by altering calcium signaling and NFAT localization. *J Immunol*. 2010;185:2836-2846.
6. Suguro M, Tagawa H, Kagami Y, et al. Expression profiling analysis of the CD5+ diffuse large B-cell lymphoma subgroup: development of a CD5 signature. *Cancer Sci*. 2006;97:868-874.
7. Narayan G, Bourdon V, Chaganti S, et al. Gene dosage alterations revealed by cDNA microarray analysis in cervical cancer: identification of candidate amplified and overexpressed genes. *Genes Chromosomes Cancer*. 2007;46:373-384.
8. Sagredo AI, Sagredo EA, Cappelli C, et al. TRPM4 regulates Akt/GSK3-beta activity and enhances beta-catenin signaling and cell proliferation in prostate cancer cells. *Mol Oncol*. 2018;12:151-165.
9. Sagredo AI, Sagredo EA, Pola V, et al. TRPM4 channel is involved in regulating epithelial to mesenchymal transition, migration, and invasion of prostate cancer cell lines. *J Cell Physiol*. 2019;234:2037-2050.
10. Berg KD, Soldini D, Jung M, et al. TRPM4 protein expression in prostate cancer: a novel tissue biomarker associated with risk of biochemical recurrence following radical prostatectomy. *Virchows Arch*. 2016;468:345-355.
11. Ashida S, Nakagawa H, Katagiri T, et al. Molecular features of the transition from prostatic intraepithelial neoplasia (PIN) to prostate cancer: genome-wide gene-expression profiles of prostate cancers and PINs. *Cancer Res*. 2004;64:5963-5972.
12. Liu P, Ramachandran S, Ali Seyed M, et al. Sex-determining region Y box 4 is a transforming oncogene in human prostate cancer cells. *Cancer Res*. 2006;66:4011-4019.
13. Singh J, Manickam P, Shmoish M, et al. Annotation of androgen dependence to human prostate cancer-associated genes by microarray analysis of mouse prostate. *Cancer Lett*. 2006;237:298-304.
14. Liu Z, Xiang Y, Sun G. The KCTD family of proteins: structure, function, disease relevance. *Cell Biosci*. 2013;3:45.
15. Bayon Y, Trinidad AG, de la Puerta ML, et al. KCTD5, a putative substrate adaptor for cullin3 ubiquitin ligases. *FEBS J*. 2008;275:3900-3910.
16. Rutz N, Heilbronn R, Weger S. Interactions of cullin3/KCTD5 complexes with both cytoplasmic and nuclear proteins: Evidence for a role in protein stabilization. *Biochem Biophys Res Commun*. 2015;464:922-928.
17. Dementieva IS, Tereshko V, McCrossan ZA, et al. Pentameric assembly of potassium channel tetramerization domain-containing protein 5. *J Mol Biol*. 2009;387:175-191.

18. Pfeiffenberger C, Allada R. Cul3 and the BTB adaptor insomniac are key regulators of sleep homeostasis and a dopamine arousal pathway in Drosophila. *PLoS Genet*. 2012;8:e1003003.
19. Stavropoulos N, Young MW. Insomniac and Cullin-3 regulate sleep and wakefulness in Drosophila. *Neuron*. 2011;72:964-976.
20. Alvarez A, Uribe F, Canales J, et al. KCTD5 and ubiquitin proteasome signaling are required for helicobacter pylori adherence. *Front Cell Infect Microbiol*. 2017;7:450.
21. Pfaffl MW. A new mathematical model for relative quantification in real-time RT-PCR. *Nucleic Acids Res*. 2001;29:e45.
22. Kodama Y, Hu CD. An improved bimolecular fluorescence complementation assay with a high signal-to-noise ratio. *Biotechniques*. 2010;49:793-805.
23. Shyu YJ, Liu H, Deng X, Hu CD. Identification of new fluorescent protein fragments for bimolecular fluorescence complementation analysis under physiological conditions. *Biotechniques*. 2006;40:61-66.
24. Gibson DG, Young L, Chuang RY, Venter JC, Hutchison CA 3rd, Smith HO. Enzymatic assembly of DNA molecules up to several hundred kilobases. *Nat Methods*. 2009;6:343-345.
25. Young JA, Sermwittayawong D, Kim HJ, et al. Fas-associated death domain (FADD) and the E3 ubiquitin-protein ligase TRIM21 interact to negatively regulate virus-induced interferon production. *J Biol Chem*. 2011;286:6521-6531.
26. Zurek N, Sparks L, Voeltz G. Reticulon short hairpin transmembrane domains are used to shape ER tubules. *Traffic*. 2011;12:28-41.
27. Albarran L, Lopez JJ, Amor NB, et al. Dynamic interaction of SARAF with STIM1 and Orai1 to modulate store-operated calcium entry. *Sci Rep*. 2016;6:24452.
28. Guo J, She J, Zeng W, Chen Q, Bai XC, Jiang Y. Structures of the calcium-activated, non-selective cation channel TRPM4. *Nature*. 2017;552:205-209.
29. Hopf TA, Scharfe CP, Rodrigues JP, et al. Sequence co-evolution gives 3D contacts and structures of protein complexes. *eLife*. 2014;3:e03430.
30. Dominguez C, Boelens R, Bonvin AM. HADDOCK: a protein-protein docking approach based on biochemical or biophysical information. *J Am Chem Soc*. 2003;125:1731-1737.
31. Gray JJ, Moughon S, Wang C, et al. Protein-protein docking with simultaneous optimization of rigid-body displacement and side-chain conformations. *J Mol Biol*. 2003;331:281-299.
32. Cerda O, Caceres M, Park KS, et al. Casein kinase-mediated phosphorylation of serine 839 is necessary for basolateral localization of the Ca(2+)-activated non-selective cation channel TRPM4. *Pflugers Arch*. 2015;467:1723-1732.
33. Blanco C, Morales D, Mogollones I, et al. EB1- and EB2-dependent anterograde trafficking of TRPM4 regulates focal adhesion turnover and cell invasion. *FASEB J*. 2019;33:9434-9452.
34. Sakaguchi T, Kikuchi Y, Kuroiwa A, Takeda H, Stainier DY. The yolk syncytial layer regulates myocardial migration by influencing extracellular matrix assembly in zebrafish. *Development*. 2006;133:4063-4072.
35. Colombo A, Palma K, Armijo L, et al. Daam1a mediates asymmetric habenular morphogenesis by regulating dendritic and axonal outgrowth. *Development*. 2013;140:3997-4007.
36. Essner JJ, Amack JD, Nyholm MK, Harris EB, Yost HJ. Kupffer's vesicle is a ciliated organ of asymmetry in the zebrafish embryo that initiates left-right development of the brain, heart and gut. *Development*. 2005;132:1247-1260.
37. Fredriksson S, Gullberg M, Jarvius J, et al. Protein detection using proximity-dependent DNA ligation assays. *Nat Biotechnol*. 2002;20:473-477.
38. Nilius B, Prenen J, Tang J, et al. Regulation of the Ca2+ sensitivity of the nonselective cation channel TRPM4. *J Biol Chem*. 2005;280:6423-6433.
39. Syam N, Rougier JS, Abriel H. Glycosylation of TRPM4 and TRPM5 channels: molecular determinants and functional aspects. *Front Cell Neurosci*. 2014;8:52.
40. Woo SK, Kwon MS, Ivanov A, Geng Z, Gerzanich V, Simard JM. Complex N-glycosylation stabilizes surface expression of transient receptor potential melastatin 4b protein. *J Biol Chem*. 2013;288:36409-36417.
41. Mizoguchi T, Verkade H, Heath JK, Kuroiwa A, Kikuchi Y. Sdf1/Cxcr4 signaling controls the dorsal migration of endodermal cells during zebrafish gastrulation. *Development*. 2008;135:2521-2529.
42. Woo S, Housley MP, Weiner OD, Stainier DY. Nodal signaling regulates endodermal cell motility and actin dynamics via Rac1 and Prex1. *J Cell Biol*. 2012;198:941-952.
43. Schinke EN, Bii V, Nalla A, et al. A novel approach to identify driver genes involved in androgen-independent prostate cancer. *Mol Cancer*. 2014;13:120.
44. Mizuno H, Kitada K, Nakai K, Sarai A. PrognoScan: a new database for meta-analysis of the prognostic value of genes. *BMC Med Genomics*. 2009;2:18.
45. Rakha EA, Reis-Filho JS, Baehner F, et al. Breast cancer prognostic classification in the molecular era: the role of histological grade. *Breast Cancer Res*. 2010;12:207.
46. Haydaroglu A, Ozyigit G. *Principles and Practice of Modern Radiotherapy Techniques in Breast Cancer*. New York, NY: Springer; 2013.
47. Duffy MJ, Harbeck N, Nap M, et al. Clinical use of biomarkers in breast cancer: updated guidelines from the European Group on Tumor Markers (EGTM). *Eur J Cancer*. 2017;75:284-298.
48. Sozucan Y, Kalender ME, Sari I, et al. TRP genes family expression in colorectal cancer. *Exp Oncol*. 2015;37:208-212.
49. Gerzanich V, Woo SK, Vennekens R, et al. De novo expression of Trpm4 initiates secondary hemorrhage in spinal cord injury. *Nat Med*. 2009;15:185-191.
50. Kruse M, Pongs O. TRPM4 channels in the cardiovascular system. *Curr Opin Pharmacol*. 2014;15:68-73.
51. Kruse M, Schulze-Bahr E, Corfield V, et al. Impaired endocytosis of the ion channel TRPM4 is associated with human progressive familial heart block type I. *J Clin Invest*. 2009;119:2737-2744.
52. Liu H, Chatel S, Simard C, et al. Molecular genetics and functional anomalies in a series of 248 Brugada cases with 11 mutations in the TRPM4 channel. *PLoS ONE*. 2013;8:e54131.
53. Liu H, El Zein L, Kruse M, et al. Gain-of-function mutations in TRPM4 cause autosomal dominant isolated cardiac conduction disease. *Circ Cardiovasc Genet*. 2010;3:374-385.
54. Schattling B, Steinbach K, Thies E, et al. TRPM4 cation channel mediates axonal and neuronal degeneration in experimental autoimmune encephalomyelitis and multiple sclerosis. *Nat Med*. 2012;18:1805-1811.
55. Brockmann M, Blomen VA, Nieuwenhuis J, et al. Genetic wiring maps of single-cell protein states reveal an off-switch for GPCR signalling. *Nature*. 2017;546:307-311.
56. He H, Peng Y, Fan S, Chen Y, Zheng X, Li C. Cullin3/KCTD5 induces monoubiquitination of DeltaNp63alpha and impairs its activity. *FEBS Lett*. 2018;592:2334-2340.

57. van Bemmelen MX, Rougier JS, Gavillet B, et al. Cardiac voltage-gated sodium channel Nav1.5 is regulated by Nedd4-2 mediated ubiquitination. *Circ Res*. 2004;95:284-291.
58. Staub O, Gautschi I, Ishikawa T, et al. Regulation of stability and function of the epithelial Na+ channel (ENaC) by ubiquitination. *EMBO J*. 1997;16:6325-6336.
59. Fotia AB, Ekberg J, Adams DJ, Cook DI, Poronnik P, Kumar S. Regulation of neuronal voltage-gated sodium channels by the ubiquitin-protein ligases Nedd4 and Nedd4-2. *J Biol Chem*. 2004;279:28930-28935.
60. Schwake M, Friedrich T, Jentsch TJ. An internalization signal in ClC-5, an endosomal Cl-channel mutated in Dent's disease. *J Biol Chem*. 2001;276:12049-12054.
61. Wegierski T, Hill K, Schaefer M, Walz G. The HECT ubiquitin ligase AIP4 regulates the cell surface expression of select TRP channels. *EMBO J*. 2006;25:5659-5669.
62. Kim W, Bennett EJ, Huttlin EL, et al. Systematic and quantitative assessment of the ubiquitin-modified proteome. *Mol Cell*. 2011;44:325-340.
63. Wagner SA, Beli P, Weinert BT, et al. A proteome-wide, quantitative survey of in vivo ubiquitylation sites reveals widespread regulatory roles. *Mol Cell Proteomics*. 2011;10:M111.013284.
64. Fritzius T, Turecek R, Seddik R, et al. KCTD hetero-oligomers confer unique kinetic properties on hippocampal GABAB receptor-induced K+ currents. *J Neurosci*. 2017;37:1162-1175.
65. Rajalu M, Fritzius T, Adelfinger L, et al. Pharmacological characterization of GABAB receptor subtypes assembled with auxiliary KCTD subunits. *Neuropharmacology*. 2015;88:145-154.
66. Schwenk J, Metz M, Zolles G, et al. Native GABA(B) receptors are heteromultimers with a family of auxiliary subunits. *Nature*. 2010;465:231-235.
67. Rohacs T, Lopes CM, Michailidis I, Logothetis DE. PI(4,5)P2 regulates the activation and desensitization of TRPM8 channels through the TRP domain. *Nat Neurosci*. 2005;8:626-634.
68. Garcia-Sanz N, Valente P, Gomis A, et al. A role of the transient receptor potential domain of vanilloid receptor I in channel gating. *J Neurosci*. 2007;27:11641-11650.
69. Nilius B, Mahieu F, Prenen J, et al. The Ca2+-activated cation channel TRPM4 is regulated by phosphatidylinositol 4,5-biphosphate. *EMBO J*. 2006;25:467-478.
70. Corey DR, Abrams JM. Morpholino antisense oligonucleotides: tools for investigating vertebrate development. *Genome Biol*. 2001;2:REVIEWS1015.
71. Cheng H, Beck A, Launay P, et al. TRPM4 controls insulin secretion in pancreatic beta-cells. *Cell Calcium*. 2007;41:51-61.
72. Earley S, Waldron BJ, Brayden JE. Critical role for transient receptor potential channel TRPM4 in myogenic constriction of cerebral arteries. *Circ Res*. 2004;95:922-929.
73. Guinamard R, Demion M, Launay P. Physiological roles of the TRPM4 channel extracted from background currents. *Physiology*. 2010;25:155-164.
74. Wang H, Xu Z, Lee BH, et al. Gain-of-function mutations in TRPM4 activation gate cause progressive symmetric erythrokeratodermia. *J Invest Dermatol*. 2019;139:1089-1097.
75. Ross-Adams H, Lamb AD, Dunning MJ, et al. Integration of copy number and transcriptomics provides risk stratification in prostate cancer: a discovery and validation cohort study. *EBioMedicine*. 2015;2:1133-1144.
76. Hasegawa T, Asanuma H, Ogino J, et al. Use of potassium channel tetramerization domain-containing 12 as a biomarker for diagnosis and prognosis of gastrointestinal stromal tumor. *Hum Pathol*. 2013;44:1271-1277.
77. Li L, Duan T, Wang X, et al. KCTD12 regulates colorectal cancer cell stemness through the ERK pathway. *Sci Rep*. 2016;6:20460.
78. Kim SY, Han BK, Kim EK, et al. Breast cancer detected at screening US: survival rates and clinical-pathologic and imaging factors associated with recurrence. *Radiology*. 2017;284:354-364.
79. Lehmann BD, Pietenpol JA. Identification and use of biomarkers in treatment strategies for triple-negative breast cancer subtypes. *J Pathol*. 2014;232:142-150.
80. Roulot A, Hequet D, Guinebretiere JM, et al. Tumoral heterogeneity of breast cancer. *Ann Biol Clin*. 2016;74:653-660.
81. Turashvili G, Brogi E. Tumor heterogeneity in breast cancer. *Front Med*. 2017;4:227.

SUPPORTING INFORMATION

Additional supporting information may be found online in the Supporting Information section.

How to cite this article: Rivas J, Díaz N, Silva I, et al. KCTD5, a novel TRPM4-regulatory protein required for cell migration as a new predictor for breast cancer prognosis. *The FASEB Journal*. 2020;00:1–19. https://doi.org/10.1096/fj.201901195RRR